JOURNAL OF GEOPHYSICAL RESEARCH, VOL. 107, NO. D20, 8279, doi:10.1029/2001JD000937, 2002

Tracer-based determination of vortex descent in the 1999/2000 Arctic winter

Jeffery B. Greenblatt[1,2] Hans-Jürg Jost,[1,3] Max Loewenstein,[1] James R. Podolske,[1] Dale F. Hurst,[4,5] James W. Elkins,[4] Sue M. Schauffler,[6] Elliot L. Atlas,[6] Robert L. Herman,[7] Christopher R. Webster,[7] T. Paul Bui,[1] Fred L. Moore,[4,5] Eric A. Ray,[5,8] Samuel Oltmans,[4] Holger Vömel,[4,5] Jean-François Blavier,[7] Bhaswar Sen,[7] Robert A. Stachnik,[7] Geoffrey C. Toon,[7] Andreas Engel,[9] Melanie Müller,[9] Ulrich Schmidt,[9] Holger Bremer,[10] R. Bradley Pierce,[11] Björn-Martin Sinnhuber,[12,13] Martyn Chipperfield,[12] and Franck Lefèvre[14]

Received 11 June 2001; revised 23 October 2001; accepted 30 October 2001; published 2 October 2002.

[1] A detailed analysis of available in situ and remotely sensed N_2O and CH_4 data measured in the 1999/2000 winter Arctic vortex has been performed in order to quantify the temporal evolution of vortex descent. Differences in potential temperature (θ) among balloon and aircraft vertical profiles (an average of 19–23 K on a given N_2O or CH_4 isopleth) indicated significant vortex inhomogeneity in late fall as compared with late winter profiles. A composite fall vortex profile was constructed for 26 November 1999, whose error bars encompassed the observed variability. High-latitude extravortex profiles measured in different years and seasons revealed substantial variability in N_2O and CH_4 on θ surfaces, but all were clearly distinguishable from the first vortex profiles measured in late fall 1999. From these extravortex-vortex differences we inferred descent prior to 26 November: as much as 397 ± 15 K (1σ) at 30 ppbv N_2O and 640 ppbv CH_4, and falling to 28 ± 13 K above 200 ppbv N_2O and 1280 ppbv CH_4. Changes in θ were determined on five N_2O and CH_4 isopleths from 26 November through 12 March, and descent rates were calculated on each N_2O isopleth for several time intervals. The maximum descent rates were seen between 26 November and 27 January: 0.82 ± 0.20 K/day averaged over 50–250 ppbv N_2O. By late winter (26 February to 12 March), the average rate had decreased to 0.10 ± 0.25 K/day. Descent rates also decreased with increasing N_2O; the winter average (26 November to 5 March) descent rate varied from 0.75 ± 0.10 K/day at 50 ppbv to 0.40 ± 0.11 K/day at 250 ppbv. Comparison of these results with observations and models of descent in prior years showed very good overall agreement. Two models of the 1999/2000 vortex descent, SLIMCAT and REPROBUS, despite θ offsets with respect to observed profiles of up to 20 K on most tracer isopleths, produced descent rates that agreed very favorably with the inferred rates from observation. *INDEX TERMS:* 3334 Meteorology and Atmospheric Dynamics: Middle atmosphere dynamics (0341, 0342); 0341 Atmospheric Composition and Structure: Middle atmosphere—constituent transport and chemistry (3334); *KEYWORDS:* N_2O, CH_4, polar vortex, subsidence, descent, stratosphere

Citation: Greenblatt, J. B., et al., Tracer-based determination of vortex descent in the 1999/2000 Arctic winter, *J. Geophys. Res.*, *107*(D20), 8279, doi:10.1029/2001JD000937, 2002.

[1]NASA Ames Research Center, Moffett Field, California, USA.
[2]Now at Program in Atmospheric and Oceanic Sciences, Princeton University, Princeton, New Jersey, USA.
[3]Bay Area Environmental Research Institute, Sonoma, California, USA.
[4]NOAA Climate Monitoring and Diagnostics Laboratory, Boulder, Colorado, USA.
[5]Cooperative Institute for Research in Environmental Sciences, University of Colorado, Boulder, Colorado, USA.
[6]National Center for Atmospheric Research, Boulder, Colorado, USA.
[7]Jet Propulsion Laboratory, California Institute of Technology, Pasadena, California, USA.
[8]NOAA Aeronomy Laboratory, Boulder, Colorado, USA.
[9]Institut für Meteorologie und Geophysik, J. W. Goethe-Universität, Frankfurt, Germany.
[10]Institute of Environmental Physics, University of Bremen, Bremen, Germany.
[11]NASA Langley Research Center, Hampton, Virginia, USA.
[12]School of the Environment, University of Leeds, Leeds, UK.
[13]Now at Institute of Environmental Physics, University of Bremen, Bremen, Germany.
[14]Service d'Aeronomie, Université Pierre et Marie Curie, Paris, France.

0148-0227/02/2001JD000937$09.00

1. Introduction

[2] Each fall, decreasing polar sunlight triggers a series of events resulting in increased circumpolar winds, the formation of an isolated region of stratospheric air known as the polar vortex, and the subsidence or diabatic descent of the vortex air column by several kilometers resulting from radiative cooling [*Schoeberl and Hartmann*, 1991; *McIntyre*, 1992]. Quantifying vortex descent is necessary if one is to understand chemical processes, such as ozone loss, occurring within the vortex, as it is otherwise difficult to differentiate between chemical and dynamical changes in ozone.

[3] Quantitative studies of vortex descent have been carried out in the past. Tracers such as N_2O, CH_4, HF, CO, HCN, and CCl_2F_2 have been used to tag similar air masses when comparing measurements made at different times and locations, and from these differences, descent has been inferred in the Arctic [*Loewenstein et al.*, 1990; *Schmidt et al.*, 1991; *Schoeberl et al.*, 1992; *Toon et al.*, 1992; *Bauer et al.*, 1994; *Emmons et al.*, 1994; *Traub et al.*, 1995; *Abrams et al.*, 1996a; *Müller et al.*, 1996, 1997; *Hartmann et al.*, 1997; *Manney et al.*, 1999] and Antarctic [*Loewenstein et al.*, 1989; *Toon et al.*, 1989; *Schoeberl et al.*, 1992, 1995; *Russell et al.*, 1993a; *Crewell et al.*, 1995; *Abrams et al.*, 1996b; *Manney et al.*, 1999; *Allen et al.*, 2000; *Kawamoto and Shiotani*, 2000]. A number of models have also been used to estimate descent [*Schoeberl et al.*, 1992; *Fisher et al.*, 1993; *Manney et al.*, 1994, 1995, 1999; *Rosenfield et al.*, 1994; *Strahan et al.*, 1994, 1996; *Bacmeister et al.*, 1995; *Eluszkiewicz et al.*, 1995; *Lucic et al.*, 1999]. Models have many advantages, including the ability to simulate the stratosphere in areas where measurements are unavailable. However, it is essential that such models be compared with observational results to validate their performance.

[4] Satellite observations are extremely useful for this goal, as satellites offer near-continuous measurement and coverage over significant portions of Earth. However, they also suffer from some major drawbacks, such as low horizontal (>100 km) and vertical (~2 km) resolution, and for all solar occultation-based instruments, limited coverage at high latitudes during the winter months. While the horizontal resolution is not particularly important for characterizing descent, which affects the vortex as a whole, the vertical resolution can be comparable to the amount of descent for short (less than ~1 month) time periods. The inability to view polar latitudes during winter also hampers observations inside the vortex, which is typically located poleward of 60°N or south. In the Arctic, stratospheric conditions sometimes displace the vortex away from the pole during portions of the winter, allowing plentiful observations inside the vortex [e.g., *Müller et al.*, 1997; *Manney et al.*, 1999]. However, these conditions are not necessarily frequent in each winter, as was the case during much of 1999/2000.

[5] Field-based observations (consisting of aircraft- and balloon-based in situ and remote sensing measurements, as well as ground-based remote observations) offer the advantages over satellite observations of high spatial resolution, especially for in situ measurements, and greater vortex penetration in winter months. However, they also suffer from several limitations, namely a lack of temporal coverage (field campaigns are expensive, and weather limits both balloon and aircraft frequency), spatial coverage (there are a limited number of polar locations suitable for airborne research), and altitude (the ER-2 aircraft is limited to ~20 km, and balloons are limited to ~30 km). Thus there is no instrument/platform combination that provides ideal vortex coverage.

[6] In order to study descent within the Arctic vortex during the 1999/2000 winter season, we have combined tracer observations from ten different instruments deployed as part of the Stratospheric Aerosol and Gas Experiment III (SAGE III) Ozone Loss and Validation Experiment (SOLVE) and the Third European Stratospheric Experiment on Ozone 2000 (THESEO 2000) campaigns. These measurements represent a variety of techniques and covered large portions of the vortex from late November 1999 through mid-March 2000. In addition, measurements from three other instruments deployed in prior years were examined to help determine a vortex starting profile. Our inferred descent rates were compared with those from previous studies of Arctic descent. Last, our descent rates were compared with results from two stratospheric chemical transport models that simulated vortex descent for 1999/2000.

2. Data and Methods

[7] In this paper, we focus on the stratospheric tracers N_2O and CH_4, which were measured by a large number of instruments during the SOLVE and THESEO 2000 campaigns. These tracers have long photochemical lifetimes (years to decades) in the middle and lower stratosphere and thus were ideal for studies of polar descent within the stratosphere, where transport timescales are on the order of months to years [*Brasseur and Solomon*, 1995].

[8] Potential temperature (θ) was chosen as the vertical coordinate because, unlike altitude or pressure, it is conserved under adiabatic displacements. In the absence of mixing, changes in θ are due exclusively to diabatic heating, which is the effect we seek to quantify. To calculate θ, measurements of temperature and pressure are needed. In general, both these quantities were measured locally on the same platform as the tracer instrument; however, for some data products, assimilated pressure and temperature fields were used to generate θ.

2.1. Instruments

[9] The instruments used in this study are listed in Table 1, along with platform, launch location, utilized data (N_2O, CH_4, θ), and flight dates. The raw data are publicly available from either the SOLVE or THESEO 2000 Web sites (http://cloud1.arc.nasa.gov/solve and http://www.nilu.no/projects/theseo2000/, respectively).

[10] The in situ balloon instruments will be discussed first. The Lightweight Airborne Chromatograph Experiment (LACE) determined the volume mixing ratios (VMRs) of eight gases including N_2O by gas chromatography (GC) with a time resolution of 70 s [*Moore et al.*, 2002]. Pressure and temperature associated with the LACE flights were measured by the Jet Propulsion Laboratory (JPL) Ozone

Table 1. Instruments Used in This Study

Instrument	Platform	Location[a]	Data Utilized			Date(s) (YYYY.MM.DD)
			N_2O	CH_4	θ	
Measurements From SOLVE/THESEO 2000						
LACE	OMS in situ[b]	Esrange	Y	Y		1999.11.19, 2000.03.05
JPL ozone	OMS in situ[b]	Esrange			Y	1999.11.19
NOAA hygrometer	OMS in situ[b]	Esrange			Y	2000.03.05
BONBON	TRIPLE[b]	Esrange	Y	Y	Y	2000.01.27, 2000.03.01
Argus[e]	ER-2[c]	Kiruna	Y			2000.01.20–2000.03.16
ALIAS[e]	ER-2[c]	Kiruna	Y			2000.01.20–2000.03.16
ACATS[e]	ER-2[c]	Kiruna	Y			2000.01.20–2000.03.16
WAS[e]	ER-2[c]	Kiruna	Y			2000.01.20–2000.03.16
MMS	ER-2[c]	Kiruna			Y	2000.01.20–2000.03.16
MkIV	OMS remote[b]	Esrange	Y	Y	Y	1999.12.03
SLS	OMS remote[b]	Esrange	Y		Y	1999.12.03
ASUR	DC-8[c]	Kiruna	Y		Y	1999.11.30–2000.03.15
HALOE	UARS[c]	n/a		Y	Y	1999.10.01–2000.03.31
Additional Measurements From Prior Years						
BONBON	CNES[b]	Esrange	Y	Y	Y	1991.11.30
ATMOS	ATLAS-2[d]	n/a	Y	Y	Y	1993.04.08–1993.04.16,
	ATLAS-3[d]	n/a	Y	Y	Y	1994.11.03–1994.11.12
Argus	OMS in situ[b]	Fairbanks	Y			1997.06.30
NOAA hygrometer	OMS in situ[b]	Fairbanks			Y	1997.06.30

[a] Base locations are as follows: Esrange, Sweden (68°N, 20°E); Kiruna, Sweden (68°N, 21°E); Fairbanks, Alaska (65°N, 148°W).
[b] Balloon platform was used.
[c] Aircraft platform was used.
[d] Space platform was used.
[e] Data from the four N_2O instruments on board the ER-2 (Argus, ALIAS, ACATS and WAS) were combined into a unified N_2O data product; see *Hurst et al.* [2002].

instrument [*Salawitch et al.*, 2002] on 19 November 1999, and by the National Oceanic and Atmospheric Administration (NOAA) Frost-Point Hygrometer [*Vömel et al.*, 1995] on 5 March 2000. The J. W. Goethe-Universität cryosampler (BONBON) [*Schmidt et al.*, 1987], which was located at the Forschungszentrum Jülich prior to 1996, obtained up to 16 air samples per flight; VMRs were determined via GC in the laboratory. Pressure and temperature associated with the BONBON flights were measured by sensors located on the balloon payload, and operated by the Centre National d'Études Spatiales (CNES) and J. W. Goethe-Universität/Forschungszentrum Jülich teams, respectively.

[11] Data from the four in situ ER-2 instruments that measured N_2O were combined into a unified N_2O (uN_2O) data product, following a procedure described by *Hurst et al.* [2002]. This procedure produced a self-consistent, high time resolution (3 s) N_2O data set for each SOLVE flight, using an objective method to evaluate and reduce bias among the instruments, followed by weighted averaging. The Argus spectrometer [*Jost and Loewenstein*, 1999] measured the VMRs of N_2O and CH_4 using second harmonic detection of an infrared tunable diode laser (TDL) in a multipass absorption cell, with an average time resolution of 3.2 s. The Aircraft Laser Infrared Absorption Spectrometer (ALIAS) [*Webster et al.*, 1994] is a TDL spectrometer that measured the VMRs of four gases, including N_2O and CH_4, with an average time resolution of 1.4 s. The Airborne Chromatograph for Atmospheric Trace Species IV (ACATS IV) [*Elkins et al.*, 1996; *Romashkin et al.*, 2001] determined the VMRs of eleven gases, including N_2O and CH_4, by GC with time resolution of 70 s. The Whole Air Sampler (WAS) [*Schauffler et al.*, 1999] filled up to 32 canisters per flight with ambient air, which were analyzed in the laboratory for ~27 trace gases including N_2O and CH_4 via GC. Pressure and temperature were measured on the ER-2 by the Meteorological Measurement System (MMS) instrument [*Scott et al.*, 1990].

[12] Next we will discuss the remote sensing balloon instruments. The MkIV instrument is a Fourier Transform Infrared (FTIR) spectrometer, which measured solar occultation spectra over the wavelength range 1.77–15.4 μm. A large number of atmospheric constituents were measured, including N_2O and CH_4. Vertical resolution was 2 km, with profiles reported on a 1-km vertical grid [*Toon*, 1991]. Pressure and temperature profiles, respectively, were derived from spectral fits to temperature-insensitive and temperature-sensitive CO_2 lines, assuming the CO_2 profile measured by the Harvard CO_2 instrument on board the Observations from the Middle Stratosphere (OMS) in situ gondola launched on 19 November 1999.

[13] The submillimeter-wave limb sounder (SLS) instrument recorded emission spectra of several gases; N_2O was measured near 600 GHz. The data presented here were flight averages of one or more limb scan emission spectra. Profiles were obtained from limb scan spectra using an iterative least squares fitting procedure, with a nominal vertical resolution of 2.5 km. Temperature and pressure profiles were obtained from a balloon sonde launched on the day before the flight [*Stachnik et al.*, 1992].

[14] On board the DC-8 aircraft was the airborne submillimeter radiometer (ASUR), which retrieved complete vertical profiles of several gases, including N_2O, every ~2000–6000 s from pressure-broadened emission lines at 652.833 GHz. The vertical resolution was 5–10 km, with profiles calculated on a 2-km vertical grid. Flight track data containing temperature and pressure for calculating θ were provided by the NASA Goddard Data Assimilation Office (DAO) [*von König et al.*, 2000].

[15] Data from two spaceborne instruments were used in this paper. The Halogen Occultation Experiment (HALOE) instrument is located on the Upper Atmosphere Research Satellite (UARS), and uses solar occultation to measure vertical profiles of several gases, including CH_4. The data used here were level 2, version 19. The instrument vertical resolution was 1.6 km at the Earth's limb, and the altitude range extended from 15 km to more than 60 km. Latitudinal coverage was from 80°S to 80°N over the course of one year. Because of the HALOE orbit and the Earth-Sun geometry during the Arctic winter months, the maximum northern coverage was limited to ~50°N from November 1999 through January 2000, and up to ~65°N in October 1999 and February–March 2000. As a result, data throughout most of the winter were limited to extravortex regions. Temperature and pressure were determined by spectral fitting of the 2.8 μm CO_2 band [*Russell et al.*, 1993b] above 35 km (10 mbar); below this altitude, they were obtained *via* interpolation from the National Meteorological Center (NMC) assimilated data product.

[16] The Atmospheric Trace Molecule Spectroscopy (ATMOS) instrument is an FTIR spectrometer similar to MkIV, which has flown on several Space Shuttle missions. ATMOS measured the abundances of ~30 gases, including N_2O and CH_4, from 12–80 km altitude with a vertical resolution of 2–3 km. Version 3 data were used here. Northern latitude coverage ranged up to 69°N during the second Atmospheric Laboratory for Applications and Science (ATLAS-2) mission (8–16 April 1993), and up to 49°N during the ATLAS-3 mission (3–12 November 1994) [*Gunson et al.*, 1996]. Pressure and temperature were determined by spectral fitting of the CO_2 absorption bands [*Stiller et al.*, 1995].

2.2. Data Selection

[17] Data were screened prior to use to determine their quality, based on the following criteria: calibration against known standards such as the NOAA Climate Monitoring and Diagnostics Laboratory (CMDL) reference gases, the existence of intercomparison with other instruments [e.g., *Chang et al.*, 1996; *Herman et al.*, 1998; *Michelsen et al.*, 1999; *Toon et al.*, 1999; *Moore et al.*, 2002], consistency of the N_2O:CH_4 correlation with other instruments when both measurements were available for a single flight, and consistency of the profiles themselves with those of other instruments. Because data from dissimilar instruments were being compared, we have used total errors, consisting of precision and accuracy estimates, as well as uncertainties of calibration gases and/or spectroscopic parameters, in our analyses.

[18] Each data point of each flight was classified as vortex, extravortex, or mixed (and therefore excluded), using one of several categorization methods. For the balloon flights, each of which did not extend over large portions of the Arctic, hemispheric maps of modified Ertel's potential vorticity (PV) [*Lait*, 1994], provided by the NASA Goddard DAO, were examined on several θ surfaces to determine vortex classification. To define the vortex edge, the Nash criterion [*Nash et al.*, 1996] was used for flights from 1999/2000 and the Argus OMS in situ flight of 30 June 1997; for the BONBON flight of 30 November 1991, the vortex edge was defined by the maximum PV gradient [*Bauer et al.*, 1994].

[19] For the unified N_2O data, flights were either classified as entirely extravortex from PV maps, or they were filtered to retain only vortex segments using the technique recently described by *Greenblatt et al.* [2002]. This technique used N_2O versus θ profiles measured inside the vortex to accurately determine the inner edge of the vortex boundary region; the inner edge was used to remove both large-scale flight segments of extravortex air, as well as small filaments of mixed composition.

[20] For the ASUR data, PV was converted to equivalent latitude (EqL) [*Butchart and Remsberg*, 1986] and points between 70°N and 90°N EqL were assumed to be inside the vortex. A comparison of the different months during 1999/2000 when the ASUR instrument was deployed showed that the vortex edge was located between 50° N and 70° N EqL. Each flight used consisted of one or more profiles measured inside the vortex, from which a single weighted average profile was constructed.

[21] HALOE data were filtered using a rotation/strain diagnostic called Q, which was integrated along rotational streamlines, with the vortex edge being defined as the rotational streamline with integrated Q of zero [*Fairlie et al.*, 1999; *Pierce et al.*, 2002]. The data were further constrained to the high midlatitudes (>45°N). Due to the small amount of data available at these latitudes, monthly average extravortex profiles were used for this paper. PV and Q were obtained from the United Kingdom Meteorological Office (UKMO) UARS assimilated wind and temperature fields [*Swinbank and O'Neill*, 1994].

[22] The ATMOS tracer data were sorted according to isentropic maps of PV and VMRs of CH_4, HNO_3, O_3, and N_2O. Averages included profiles with similar tracer distributions throughout the altitude range considered within selected geographic regions. Profiles displaying inversions (e.g., regions where θ was not single-valued with respect to tracer VMR) were excluded from the averages. Classifications (vortex and midlatitude extravortex) were confirmed by comparison with tracer:tracer correlations [*Michelsen et al.*, 1998a, 1998b].

2.3. Binning and Inversion

[23] Filtered data were binned into 5 K θ intervals in order to facilitate comparison among data sets. The tracer VMR reported for each θ bin was calculated from the weighted mean of all data within the bin. Gaps in the data were filled in using linear interpolation.

[24] For the purpose of comparing changes in θ on N_2O or CH_4 surfaces of constant VMR (isopleths), the data were "inverted" so that θ could be expressed as a function of tracer VMR. Inverted data were binned in intervals of 10 parts per billion by volume (ppbv) N_2O and 40 ppbv CH_4. The resulting tracer-binned data were calculated as follows: all data points whose VMR value ±1 standard deviation (σ) fell within a given tracer bin were considered in the calculation for that bin, and the minimum and maximum θ of all qualifying points were determined. The θ for the tracer-binned data point was defined as the midpoint of this range, and the 1σ uncertainty in θ was defined as half the range. Tracer-binned data were constructed from θ-binned data, rather than raw data, primarily to overcome data sparseness for some balloon flights. Gaps in the resulting data were filled in using linear interpolation.

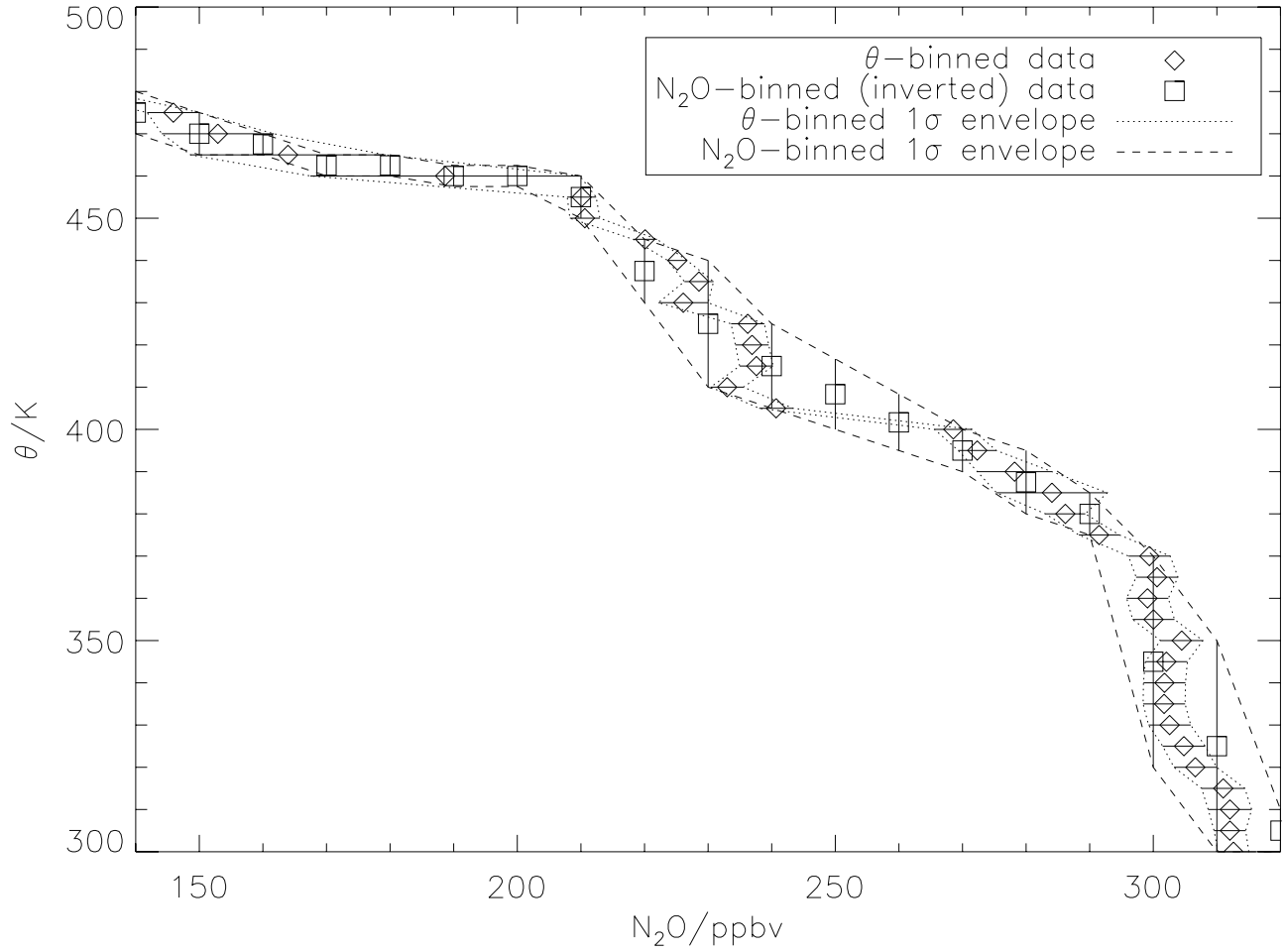

Figure 1. Illustration of the inversion technique, using part of the N_2O profile from LACE on 19 November 1999 as an example. Diamonds represent "θ-binned" data, that is, data which have been binned into 5 K θ intervals, with horizontal bars indicating ±1σ uncertainties in N_2O for each data point. Squares represent inverted "N_2O-binned" data, which have been placed into 10 ppbv N_2O intervals from the θ-binned data, with vertical bars indicating ±1σ uncertainties in θ for each data point. The ±1σ envelopes of the N_2O-binned data (dashed line) generally encompassed those of the θ-binned data (dotted line), which indicates that this approach provides a conservative estimate of the uncertainty relative to θ. The overestimate of the N_2O-binned envelope with respect to the θ-binned envelope between 250 and 260 ppbv N_2O was due to a lack of any θ-binned data points in these two N_2O bins; the interpolation scheme smoothly filled in this region from surrounding data.

[25] Figure 1 illustrates this idea, using a portion of the LACE N_2O profile of 19 November 1999 as an example. The region from 150–210 ppbv illustrates the need to consider the N_2O uncertainties in the calculation of θ for a given tracer bin, because N_2O error bars in this region were much larger than the 10-ppbv bin size, and therefore single data points contributed to the calculation of θ in several bins. Within the 230 and 240 ppbv N_2O bins, where the θ-binned data display an inversion with respect to N_2O, and at 300 ppbv and above, where the θ-binned data became essentially vertical, the midpoint of the range of θ values within a bin served as the most useful definition of θ. The ±1σ envelopes of the N_2O-binned data (dashed line) generally encompassed those of the θ-binned data (dotted line), which indicates that this approach provides a conservative estimate of the uncertainty relative to θ. The overestimate of the N_2O-binned envelope with respect to the θ-binned envelope between 250 and 260 ppbv N_2O was due to the lack of any θ-binned data points in these two N_2O bins; the interpolation scheme smoothly filled in this region from surrounding data.

2.4. Models

[26] SLIMCAT is a three-dimensional chemical transport model using horizontal winds and temperatures from the UKMO-UARS assimilation [*Swinbank and O'Neill*, 1994] to drive transport on an isentropic (θ-based) vertical coordinate. Vertical motion is diagnosed by calculating heating rates from a radiation model. The abundances of chemical species in the stratosphere are calculated using a detailed chemistry scheme [*Chipperfield*, 1999]. The model simulates the distribution of all species involved in stratospheric ozone depletion, as well as some trace gases, such as N_2O. The SLIMCAT model run started on 21 October 1991 and

was integrated at low resolution (7.5° × 7.5° × 18 θ levels) until November 1999. Output from this run was then used to initialize a higher resolution simulation from 3 November 1999 to 31 March 2000, on 24 θ levels ranging from 335 to 2726 K. It was assumed that an EqL greater than 70°N was inside the vortex for the entire winter, and data between 70° and 80°N EqL were used to produce vortex averages over this time period. The N_2O data were recorded daily, but for the current analysis the data were averaged over 10 day periods, and interpolated as described above in 5 K θ intervals. Data were also inverted into 10 ppbv N_2O bins. No error bars were calculated for the original data, so all data points were treated equally, and uncertainties in N_2O or θ represented the observed variation for a given θ or N_2O bin, respectively.

[27] REPROBUS is a three-dimensional chemical transport model whose advection is driven by the 6-hourly European Centre for Medium-Range Weather Forecasting (ECMWF) meteorological analysis [*Lefèvre et al.*, 1994, 1998]. The model includes a comprehensive treatment of gas-phase and heterogeneous stratospheric chemistry, as well as a semi-Lagrangian transport scheme integrated with 2° × 2° horizontal resolution, using all three components of the wind field. Calculations were performed on 42 vertical levels from the ground up to 0.1 hPa. N_2O and CH_4 tracer fields were initialized from zonal mean climatologies on 1 November 1999, and the model was run until 30 March 2000, recording N_2O and CH_4 once every 10 days. As with the SLIMCAT model, data between 70° and 80°N EqL were used to produce vortex averages, except for the two dates following the vortex break-up (20 and 30 March) when data were averaged between 80° and 90°N EqL, in order to obtain enough points within the vortex for good averaging statistics. Average tracer VMR values were calculated on 5 K θ intervals over the range 300–650 K. Data were inverted into 10 ppbv N_2O and 40 ppbv CH_4 intervals, the same as for the observational data. No error bars were originally calculated, so all data were treated equally, and uncertainties in θ represented the observed variation for a given N_2O or CH_4 bin.

3. Results and Discussion

[28] The 1999/2000 winter was characterized by unusually low stratospheric temperatures [*Manney and Sabutis*, 2000], which led to extensive PSC formation and subsequent ozone loss when sunlight returned to the vortex in mid-January [e.g., *Rex et al.*, 2002]. By early November, the vortex was fairly well established with a strong polar jet above 800 K, but a weak jet at lower levels; by early December, the vortex was established down to 465 K [*Manney and Sabutis*, 2000]. This vortex persisted until mid-April [*Waugh and Rong*, 2002]. Planetary wave activity occurred throughout the winter season, with three pulses occurring during the measurement period: late November, mid-January through early February, and early March [*Newman et al.*, 2002].

3.1. Data From SOLVE/THESEO 2000

[29] Figure 2 shows the balloon-borne data from 1999/2000. The data can be roughly divided into two groups: late fall, consisting of the 19 November LACE and 3 December MkIV and SLS profiles, and mid to late winter, consisting of the 27 January and 1 March BONBON profiles and the 5 March LACE profile. The late fall profiles lie at higher θ levels than the winter profiles over almost the entire range of N_2O and CH_4 values; these differences are a result of descent. The late fall profiles also show a larger degree of variability than the later profiles, a point that will be addressed below. The March BONBON and LACE profiles, measured four days apart and launched from the same location (Esrange, Sweden), are in very good agreement with each other for both N_2O and CH_4, with the exception of a difference seen in N_2O, which falls significantly outside the 1σ error bars beginning at 478 K. The cause of this discrepancy is not understood, but may be linked to a difference in the N_2O:CH_4 correlations of these profiles below 40 ppbv N_2O (see below). The 27 January BONBON profile lies 9 ± 6 K (1σ) above the two March profiles over 40–280 ppbv N_2O and 680–1600 ppbv CH_4; the difference is attributed to late winter descent.

[30] Figure 3 shows the unified N_2O data measured on the ER-2 in two panels, with a balloon profile shown for reference on each panel. Data are shown after binning into 5 K θ intervals for clarity. The profiles are very tight over the entire time period, with the ±1σ of N_2O within a given θ bin averaging 11.4 ppbv over the range 370–470 K, the approximate vortex altitude region sampled by the ER-2. A decrease in θ on a given N_2O level can clearly be seen over the 52-day period, and often from flight to flight.

[31] Figure 4 shows ASUR profiles in three panels. A reference in situ balloon profile is also shown for each panel to indicate how closely the ASUR data agree with in situ measurements made at comparable times. A systematic overestimation of N_2O at low VMR is apparent, which is due to the inherent limited vertical resolution of ASUR (5–10 km) and the high curvature of the profile in that region. At higher N_2O values (e.g., above ~180 ppbv), where the change in slope is more gradual, the agreement with in situ measurements is much better. We first applied the ASUR averaging kernel to the balloon and unified N_2O data, producing profiles with the same vertical resolution as ASUR. The resulting smoothed data showed much better agreement with ASUR at all N_2O levels. Although using such an approach would allow comparison below 150 ppbv, it was desirable to retain the higher vertical resolution of the other instruments. Therefore, in the analyses which follow, no such averaging was applied to the data, and only the ASUR data on the 200 and 250 ppbv N_2O isopleths were used.

3.2. N_2O:CH_4 Correlation

[32] The N_2O:CH_4 correlations for balloon data from 1999/2000 are presented in Figure 5. The five data sets show very good agreement with each other, except in the region between ~10 and 40 ppbv N_2O, where the LACE flight of 5 March differs significantly from the other data, including the two BONBON flights. The difference in the LACE correlation may indicate real differences in the N_2O:CH_4 correlation curve, because the MkIV profile of 15 March (not shown) closely follows the LACE correlation in this region. However, N_2O values below 50 ppbv were not utilized in the work presented in this paper, so the disagreement does not impact our conclusions.

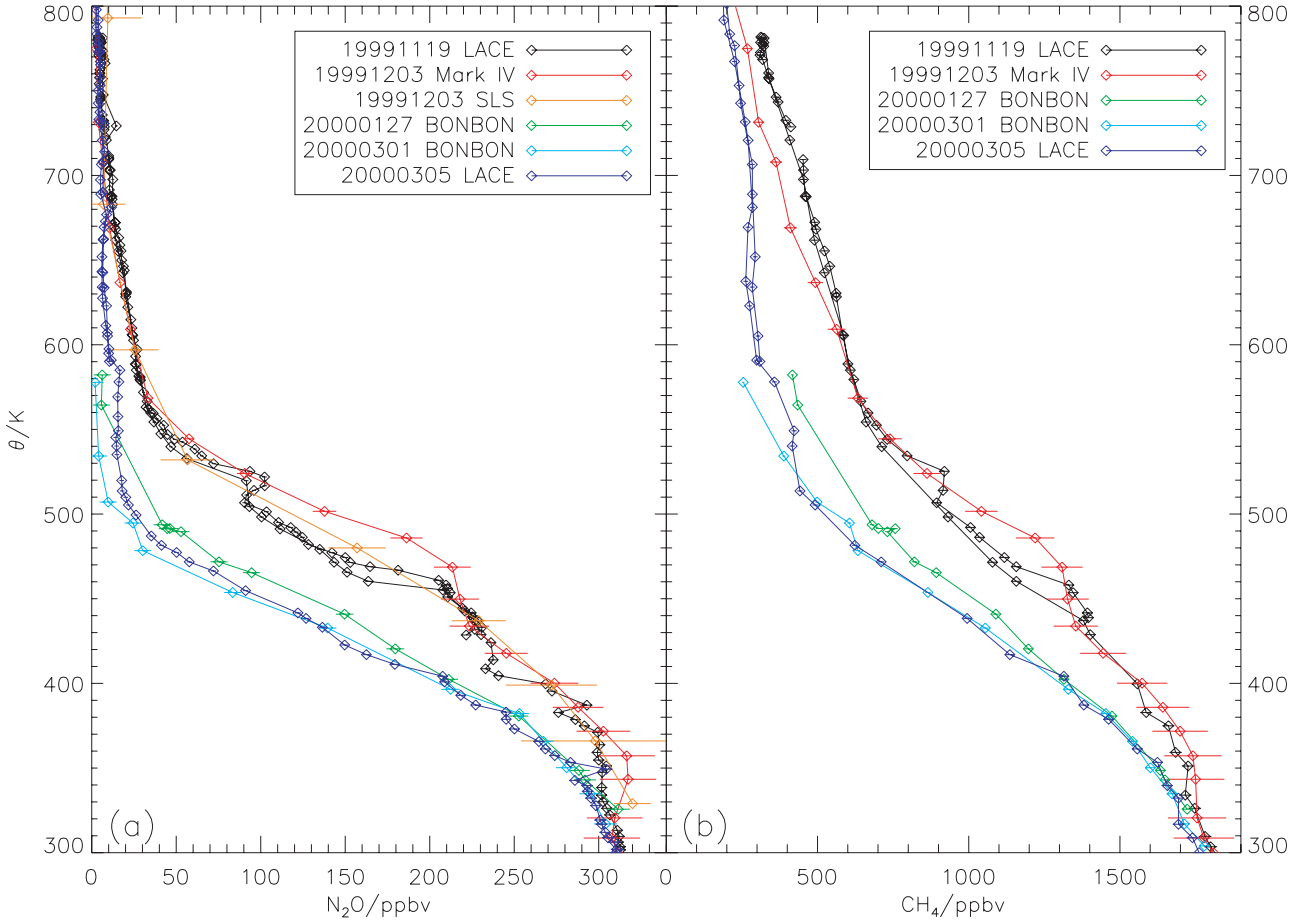

Figure 2. Balloon profiles from 1999/2000 for (a) N_2O and (b) CH_4. The legend indicates the date of each flight (YYYYMMDD format) and the instrument acronym. The color scheme is the same for both N_2O and CH_4. Note that SLS only measured N_2O. Horizontal bars indicate $\pm 1\sigma$ uncertainties of each data point. Other lines connect the points of each profile.

[33] Also shown in the figure are the ATMOS vortex and midlatitude correlations [*Michelsen et al.*, 1998a], constructed from measurements made from 1992 to 1994. The data from 1999/2000 fall in between the two ATMOS correlations between ~30 and 150 ppbv N_2O, and fall at higher CH_4 values above ~170 ppbv N_2O. The secular trends in N_2O and CH_4 [*Intergovernmental Panel on Climate Change* (*IPCC*), 1996] are responsible for most of the differences at high N_2O (i.e., lower altitudes), but at lower N_2O values the influence of tropospheric trends is expected to be smaller because of the shorter photochemical lifetimes N_2O and CH_4. The lack of sensitivity to such trends at these altitudes is supported by the excellent agreement between ATMOS correlations from 1994 and MkIV and ALIAS II correlations from 1997 [*Herman et al.*, 1998]. The differences shown in Figure 5 are consistent with differences between the ATMOS early fall developing vortex (or protovortex) and extravortex correlations reported by *Manney et al.* [2000]. Such a difference can be attributed to some descent followed by mixing of extravortex air into the vortex, which is expected during this time of year [*Manney et al.*, 2000; *Plumb et al.*, 2000]. The differences, however, are not as substantial as those between the extravortex correlation and the correlation observed in the spring vortex in 1993 (the ATMOS vortex curve in Figure 5). These differences have similarly been attributed to significant unmixed descent followed by mixing with extravortex air [*Michelsen et al.*, 1998a, 1998b, 1999].

[34] For the purposes of this paper, it was not necessary to understand why the N_2O:CH_4 correlation for the 1999/2000 winter differed from the ATMOS correlations, because the correlation was only needed to compare descent on N_2O and CH_4 isopleths. Thus a piecewise, weighted least squares fit was generated, based on the five balloon flights, between 700 and 1800 ppbv CH_4 (44–323 ppbv N_2O). This fit is shown in Figure 5, with its functional form listed in the caption. The fit was used to generate the CH_4 isopleths corresponding to the N_2O isopleths displayed in Figure 6.

3.3. Late Fall Vortex Inhomogeneity

[35] Hemispheric PV maps at 450 K show low gradients through early December 1999 [see, e.g., *Newman et al.*, 2002, Figure 11], suggesting some mixing of vortex and midlatitude air in the lower stratosphere. It is clear from examination of the three fall balloon profiles (Figure 2) and the fall ASUR data (Figure 4a) that the vortex tracer profiles were quite variable in late fall. For instance, the mean MkIV-LACE difference was 23 ± 3 K between 110 and 200 ppbv N_2O, and 20 ± 4 K between 960 and 1200 ppbv

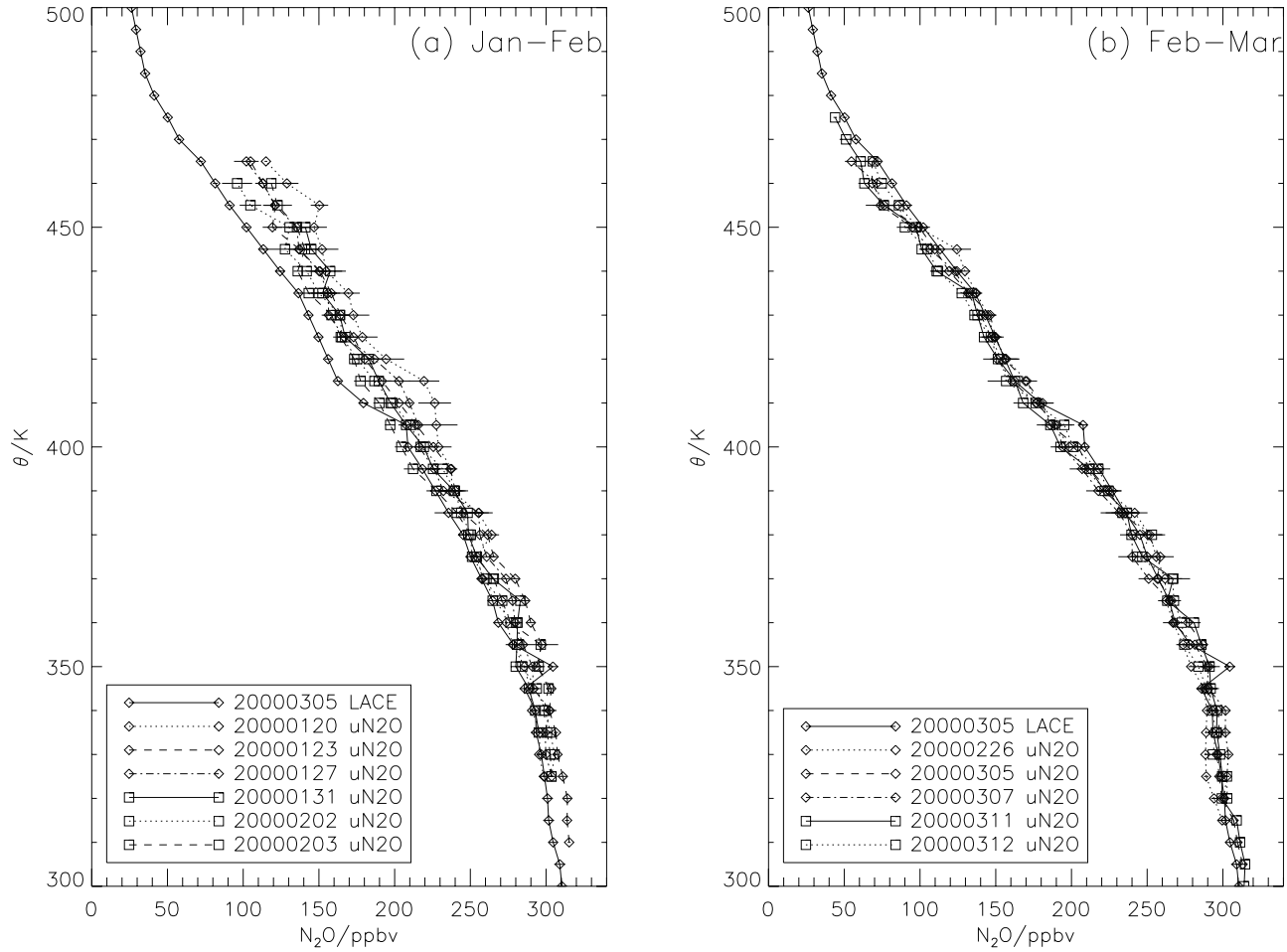

Figure 3. Unified N_2O ("uN_2O") profiles from 1999/2000 for the two ER-2 deployments: (a) 20 January to 3 February 2000 and (b) 26 February to 12 March 2000. In addition to unified N_2O data, the LACE balloon profile of 5 March 2000 (see Figure 2) is included in each panel to facilitate comparison. All data have been binned into 5 K θ intervals for clarity. Horizontal bars indicate ±1σ uncertainties, and other lines connect the points of each profile. As the ER-2 aircraft, from which unified N_2O data were measured, had a flight ceiling of ∼21 km, the data do not extend as high in θ as for the balloon measurements.

CH_4. The mean SLS-LACE difference was about half as large, 11 ± 1 K between 110 and 150 ppbv N_2O. As MkIV and SLS were flown on the same balloon payload, the differences in their measurements were likely due to the fact that the instruments observed air masses in different directions, corresponding to a horizontal separation of ∼800 km.

[36] The ASUR instrument sampled large regions of the vortex between 30 November and 16 December. For this portion of the year, the data reveal a variability, indicated by ±1σ range in θ, which was similar to the MkIV-LACE differences: 19 K at 200 ppbv N_2O and 25 K at 250 ppbv. For late winter ASUR profiles (27 February to 15 March), the variability dropped to 17 K at 200 ppbv and 11 K at 250 ppbv (excluding the flight of 8 March, which exhibited unusually high N_2O deviations; see magenta curve in Figure 4c). By comparison, the unified N_2O variability in late winter (26 February to 12 March) was 7.4 K at 200 ppbv and 9.8 K at 250 ppbv. Thus, though the noise in the ASUR data is certainly greater than for unified N_2O, particularly at 200 ppbv N_2O, the large decrease in the ASUR variability at 250 ppbv is indicative of a more homogenous vortex in late winter than late fall.

[37] Further evidence for an inhomogenous vortex is given in a study by *Ray et al.* [2002]. They found that they could explain the differences in tracer-tracer relationships between the November and March LACE profiles with a simple differential diabatic descent model. In this model, air parcels underwent different amounts of descent prior to the 19 November measurement, resulting in air with significantly different tracer VMRs on the same θ surfaces, which subsequently mixed [see, e.g., *Plumb et al.*, 2000]. Their model simultaneously fit six measured stratospheric tracers, including N_2O and CH_4, producing a self-consistent result with differential diabatic descent ranging from ∼2 km at 15 km to ∼6 km above 30 km. Thus their analysis indicated that the vortex was inhomogenous in the fall but became well mixed later in the winter.

[38] *Manney et al.* [2000] cited evidence for vortex inhomogeneity even earlier in the winter of 1994/1995. From 3–12 November 1994, the ATMOS instrument

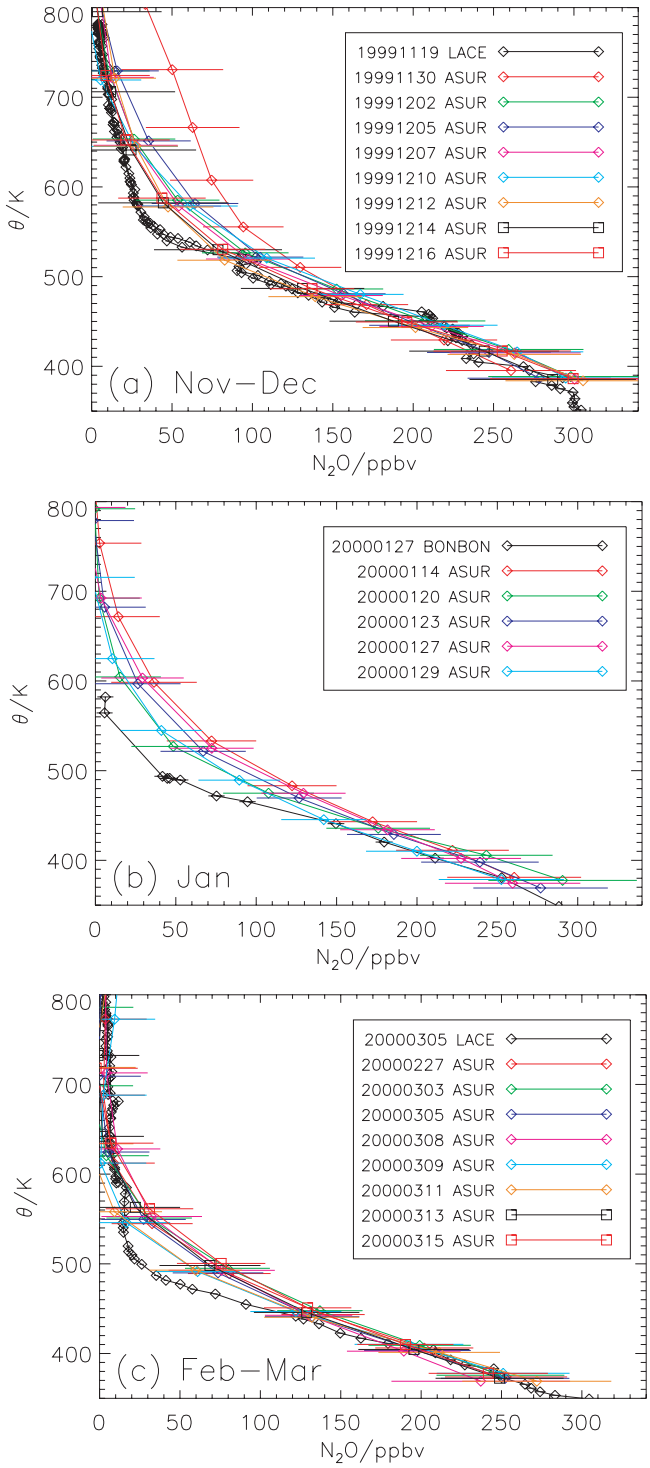

Figure 4. ASUR profiles from 1999/2000 for the three DC-8 deployments: (a) 30 November to 16 December 1999, (b) 14–29 January 2000 and (c) 27 February to 15 March 2000. In addition to ASUR data, one balloon flight from Figure 2 is included in each panel to facilitate comparison. Horizontal bars indicate ±1σ uncertainties, and other lines connect the points of each profile. The disagreement between the ASUR and balloon data for N_2O less than ~150 ppbv is due to the limited vertical resolution (~5–10 km) of the ASUR instrument, and the high curvature of the profiles in this region.

observed several laminae within the developing polar vortex whose N_2O:CH_4 correlations indicated both entrainment of tropical air, as well as midlatitude air that had undergone significant descent. The tracer versus θ profiles indicated large deviations from the bulk correlation in these regions, resulting in a vortex with substantial inhomogeneity.

[39] All of the above indicate that the vortex tends to be fairly inhomogenous in late fall. By early November, the vortex is typically well established only above 600 K [*Waugh and Randel*, 1999], and in 1999 had only recently formed in the lower stratosphere [*Manney and Sabutis*, 2000]. Thus it is a reasonable conclusion that complete mixing had not yet occurred. The smaller variability in θ for a given tracer isopleth seen later in the winter supports the idea of a more uniformly mixed vortex.

3.4. Late Fall Average Profile

[40] For the purpose of estimating an average late fall vortex profile with realistic uncertainties, we have combined the LACE and MkIV balloon profiles in the following manner. (The SLS profile was not included because of its large error bars at low and high N_2O levels. However, the SLS measurements were bounded by the other two profiles, so their omission did not detract from the goal of creating a profile that spanned the range of observations. The ASUR data were not included due to their low vertical resolution). It was not appropriate to calculate error-weighted averages because the profiles did not look at the same air parcels. Thus, for each θ bin, the minimum and maximum tracer VMR ±1σ errors were determined; the "average" VMR was defined as the midpoint of that range, and the 1σ uncertainty was defined as half the range. The procedure was applied independently to the N_2O and CH_4 data. The date assigned to each profile was the average date of the two data sets, 26 November 1999. The profiles are shown in Figure 7.

3.5. Time Series

[41] The balloon, unified N_2O and ASUR data have been combined and presented as a time series along several N_2O and CH_4 isopleths in Figure 6. Data shown here have been inverted as described in the previous section to generate θ as a function of N_2O or CH_4. The levels of 50, 100, 150, 200, and 250 ppbv N_2O were chosen to span the useful range of the measurements: at levels below 50 ppbv, there is almost no unified N_2O data, and the balloon profiles become quite steep in θ, making comparisons along isopleths difficult; much above 250 ppbv, the curves cluster on top of one another at all time periods, indicating marginal descent and probably significant mixing with midlatitude air on these isopleths [e.g., *Abrams et al.*, 1996a]. CH_4 levels of 720, 920, 1080, 1280, and 1480 ppbv were chosen to correspond approximately (to within one 40-ppbv CH_4 bin) to these N_2O levels, based on the average N_2O:CH_4 correlation derived from the balloon measurements, shown in Figure 5. Simple fits through the data (linear least squares fits in dense data regions (November–December, January–February, and February–March deployments), and connected points in between these regions) have been applied to the N_2O data to indicate the general progress of the descent throughout the winter. These same fits have been reproduced on the CH_4 panel for reference. The more limited

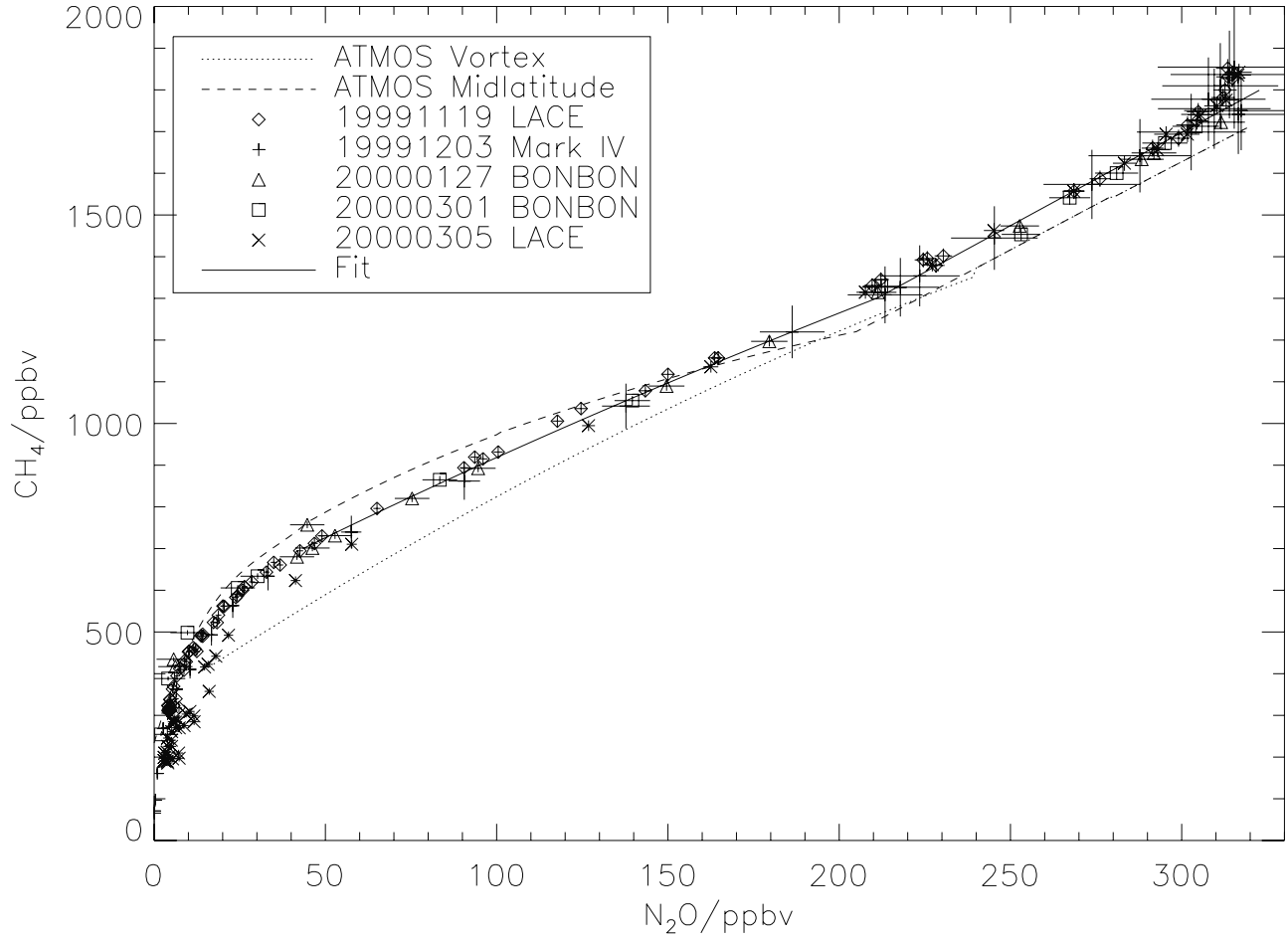

Figure 5. N_2O:CH_4 correlations for balloon flights from 1999/2000. Symbols indicate individual flights. Horizontal and vertical bars indicate ±1σ uncertainties. Shown also are ATMOS correlations for midlatitude and polar vortex air [*Michelsen et al.*, 1998a]. N_2O:CH_4 fit function is indicated by solid line, with equation $[N_2O] = p_0 + p_1[CH_4] + p_2[CH_4]^2$, where $[N_2O]$ and $[CH_4]$ are in ppbv. Coefficients p_i are defined piecewise for two CH_4 regions: $[CH_4]$ = 700–1300 ppbv, p = [−103.265, 0.172407, 5.32430 × 10^{-5}]; $[CH_4]$ = 1300–1800 ppbv, p = [−80.0715, 0.223859, 0].

CH_4 data are very consistent with these fits throughout the winter.

[42] The progress of descent is evident in detail in Figure 6. The rates of descent generally increased with decreasing tracer VMR, as indicated by the slope of the fits, and the greatest rates of descent occurred before 1 January. Between the midwinter (January–February) and late winter (February–March) data segments, the descent rates slowed considerably. Data from all instruments were in excellent agreement with each other throughout the winter, with the exception of the LACE and MkIV late fall data, which lay outside each other's error bars on the 150 ppbv N_2O and 1080 ppbv CH_4 isopleths because of the vortex inhomogeneity discussed earlier.

3.6. Vortex Starting Profile

[43] Many studies of vortex descent have calculated the total descent over the winter season starting from profiles measured in late fall [e.g., *Bauer et al.*, 1994; *Strahan et al.*, 1994; *Müller et al.*, 1996; *Hartmann et al.*, 1997]. However, it is known that descent can begin quite early in the winter season. For instance, *Michelsen et al.* [1998b] and *Manney et al.* [1999] showed that profiles measured inside the Arctic vortex during 3–12 November 1994 had already descended several km relative to extravortex profiles. *Abrams et al.* [1996a] calculated from analysis of PV contours that descent had begun in the fall of 1992 in the Arctic between 1 October and 12 November, with the earliest dates occurring at the highest altitudes (>42 km). *Rosenfield et al.* [1994] chose a starting date of 1 November for model simulations of Arctic vortex descent in 1988/1989 and 1991/1992, with significant descent rates calculated from the first day of the simulations.

[44] By 19 November 1999, the date of the first LACE profile, significant descent had occurred at all altitudes relative to extravortex profiles, as will be demonstrated shortly. Thus using this profile (or the 26 November 1999 average fall profile) as the starting point for calculating descent would miss a significant amount of descent that occurred earlier in the fall. In order to determine the total vortex descent in 1999/2000, a reasonable starting profile had to be established. Prior to vortex formation in late fall, air in polar regions is constantly mixed over horizontal distances of several thousand km [*Schoeberl and Hartmann*,

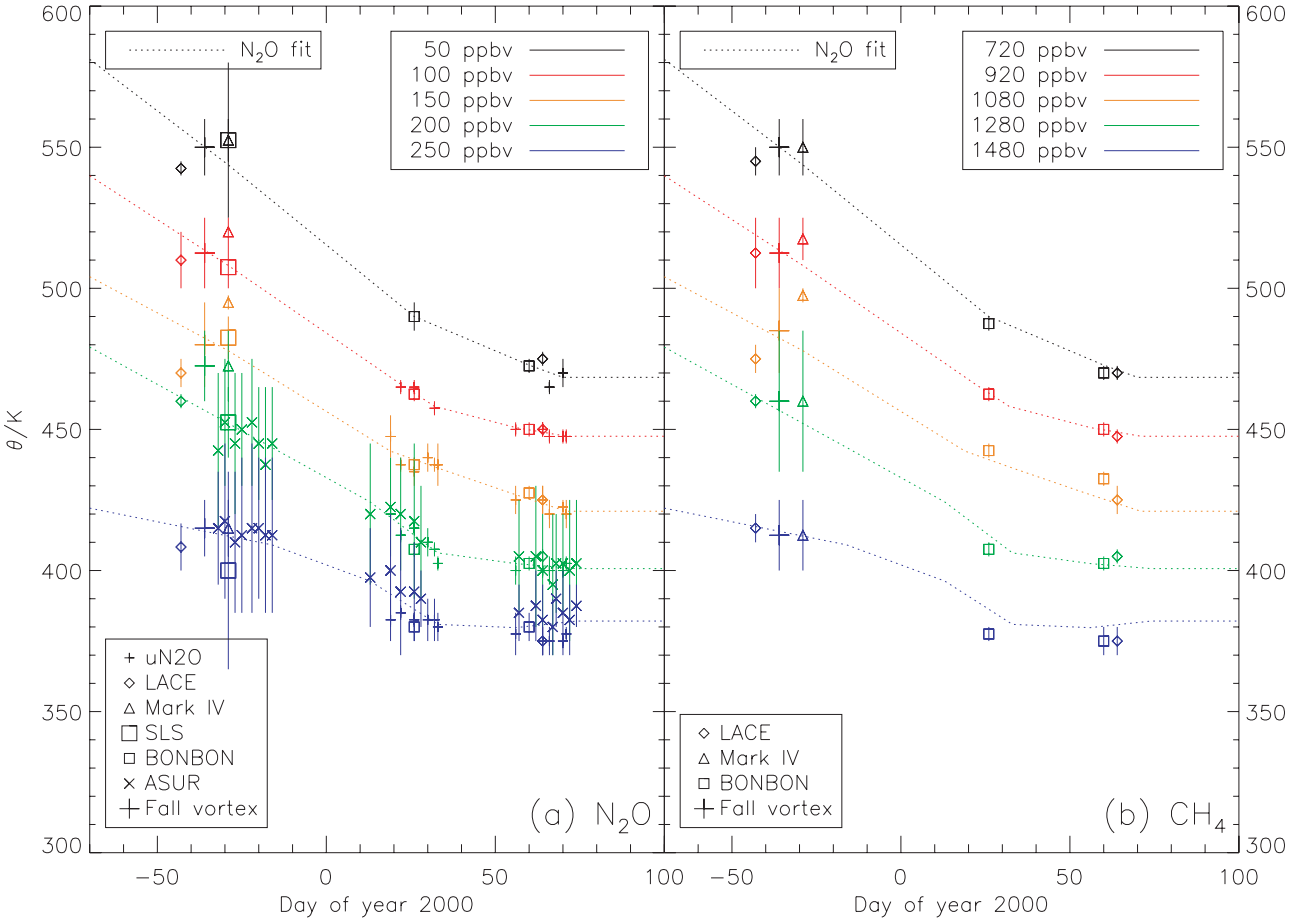

Figure 6. Descent time sequence for five (a) N_2O and (b) CH_4 isopleths. Each isopleth is denoted by a separate color. CH_4 isopleths correspond to N_2O isopleths by the equation in Figure 5. Symbols indicate individual instrument measurements. Vertical bars indicate $\pm 1\sigma$ uncertainties. Dotted lines are fits for each N_2O isopleth (fits are repeated on CH_4 panel), where linear least squares fits were made in dense data regions (November–December, January–February, and February–March deployments), and lines are connected together to span these regions. "Fall vortex" profiles (crosses), dated 26 November 1999, are constructed from averages of the 19 November LACE and 3 December MkIV profiles (see section 3.4), which are shown in their entirety on Figure 7.

1991]. Thus the tracer versus θ profile of polar air before vortex formation strongly resembles air of midlatitude composition. This has been confirmed observationally by a number of studies [*Bauer et al.*, 1994; *Abrams et al.*, 1996a; *Herman et al.*, 1998; *Jost et al.*, 1998; *Michelsen et al.*, 1998a]. It has been recognized that the tracer versus θ profiles exhibit small seasonal changes [*Abrams et al.*, 1996a], and that tropical profiles appear significantly different due to their partial isolation from the midlatitudes [e.g., *Jost et al.*, 1998; *Herman et al.*, 1998; *Michelsen et al.*, 1998a]. However, by limiting our examination to high-latitude, extravortex regions, we have assembled a selection of candidate vortex starting profiles.

[45] These profiles are shown in Figure 7, along with the 26 November 1999 average vortex profile for reference (solid black line). The extravortex profile from the BONBON instrument, shown as a solid red line, was launched from Kiruna, Sweden on 30 November 1991 [*Bauer et al.*, 1994]. Averaged extravortex profiles from the April 1993 and November 1994 ATMOS missions are shown as orange and green solid lines, respectively (H. A. Michelsen, private communication, 2001). The Argus profile, shown as a solid cyan line (for N_2O only), was measured in Fairbanks, Alaska on 30 June 1997 [*Jost et al.*, 1998]. It exhibited several large excursions to low N_2O that have been interpreted as vortex remnant filaments, and were therefore omitted from Figure 7. The limited extravortex data from 1999/2000 included a unified N_2O profile from 16 March (dark blue solid line, N_2O only), and monthly averaged HALOE profiles from December, January, and March poleward of 45°N (magenta, black, and red, respectively, with dotted lines; CH_4 only).

[46] While there is variation among profiles of up to ~70 ppbv N_2O and ~400 ppbv CH_4 on certain θ levels, the overall pattern is consistent through multiple years and seasons, and is, most importantly, quite distinct from the 26 November 1999 average vortex profile. Therefore, we assert that any profile from the set presented here can be used as a proxy for the vortex starting condition for 1999/2000. The November 1994 ATMOS average was chosen, which when both N_2O and CH_4 were considered, occupied a roughly median value at all θ values. We denoted this

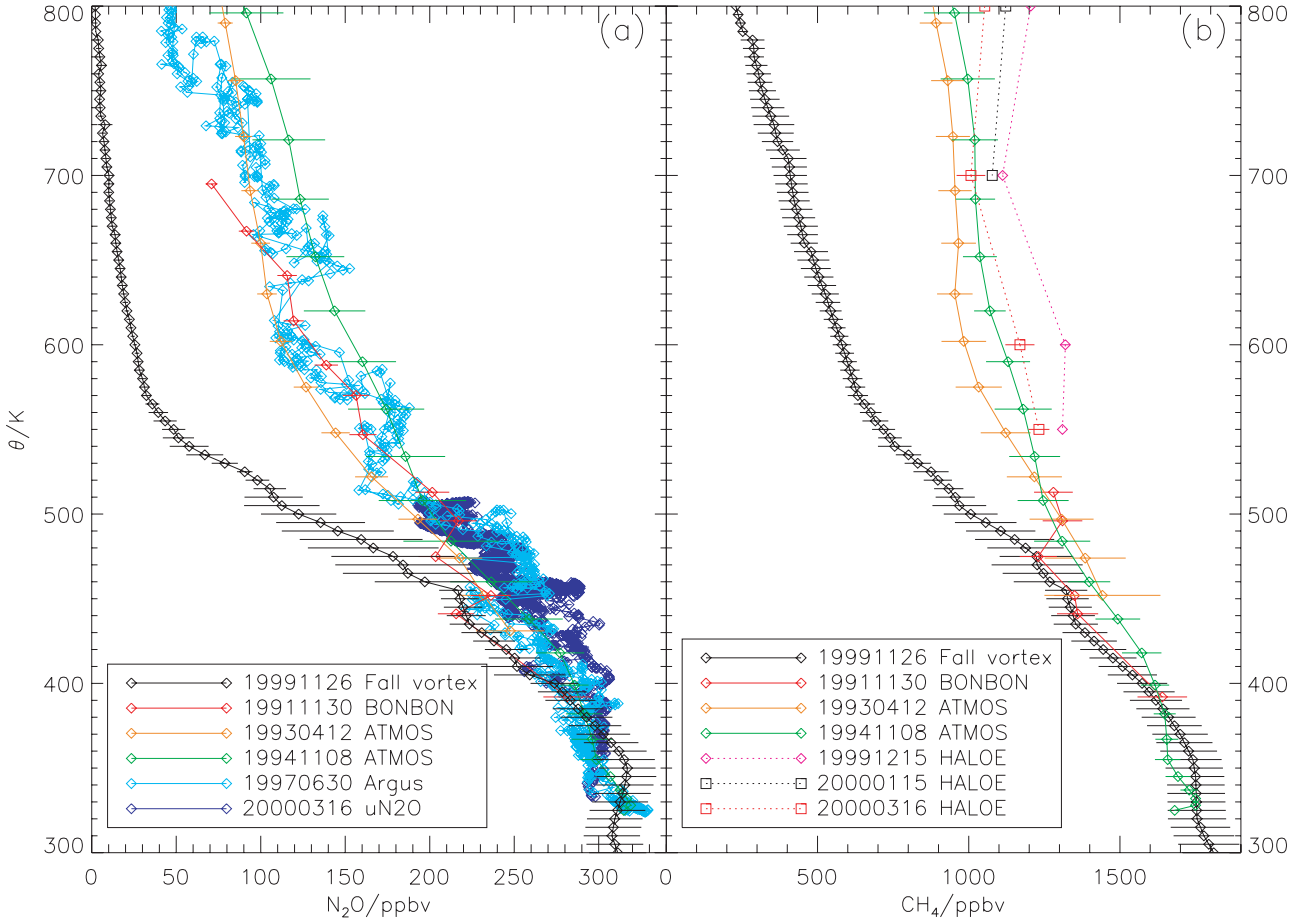

Figure 7. High-latitude, extravortex profiles from several years and seasons for (a) N_2O and (b) CH_4. Also shown for reference is the 26 November 1999 "fall vortex" profile, whose construction is explained in section 3.4. The ATMOS 1994 average profile occupies approximately a central location among extravortex profiles, when both N_2O and CH_4 are considered. This profile, denoted "START," was used as a proxy for the vortex starting profile in subsequent calculations.

profile as the "START" profile, and used it in all subsequent calculations. Note that the uncertainty associated with this profile does not represent the full range of year-to-year variations in starting profiles shown in Figure 7. Extending the uncertainties in θ to include these variations would render the starting profile useless, however, because the error bars would be larger than the differences in θ on most N_2O isopleths. Thus we have chosen to retain the original uncertainties, with the caveat that the actual change in θ for 1999/2000 may lie outside the stated error bars.

3.7. Descent Calculations

[47] In order to determine the amount of descent between measurements made at different times, differences in θ between profiles have been calculated, with the results shown in Figure 8. Vertical bars indicate ±1σ uncertainties, which were calculated as the quadrature sum of individual profile uncertainties. The diamonds/solid lines represent differences (Δθ, expressed in K) between the START profile and the 26 November 1999 average; squares/dotted lines, between the 26 November average and the 27 January 2000 BONBON profile; and triangles/dashed lines, between the BONBON profile and the 5 March 2000 LACE profile. Differences are shown for both N_2O and CH_4 data in each case.

[48] For the START to 26 November difference, Δθ ranged from 397 ± 15 K (1σ) at the lowest VMR values (30 ppbv N_2O and 640 ppbv CH_4), to 28 ± 13 K above 200 ppbv N_2O and 1280 ppbv CH_4. These differences were larger than those observed in any other profile pair, and indicated that a great amount of descent had occurred by late fall 1999. Such large descent was also inferred for early November 1994, when the ATMOS instrument examined air both inside and outside the forming polar vortex [*Michelsen et al.*, 1998b]. While that study expressed descent in terms of changes in altitude only, differences in terms of θ have been calculated and found to be comparable to our results: 220–240 K at 30 ppbv N_2O and 640 ppbv CH_4, and 380 K or more below 10 ppbv N_2O and 390 ppbv CH_4 (H. A. Michelsen, private communication, 2001).

[49] The 26 November to 27 January differences were much smaller than the START 26 November differences below 170 ppbv N_2O and 1160 ppbv CH_4, but were fairly comparable above these isopleths. From 40–280 ppbv N_2O and 680–1600 ppbv CH_4, which covered most of the tracers' dynamic ranges, Δθ was fairly constant at 54 ±

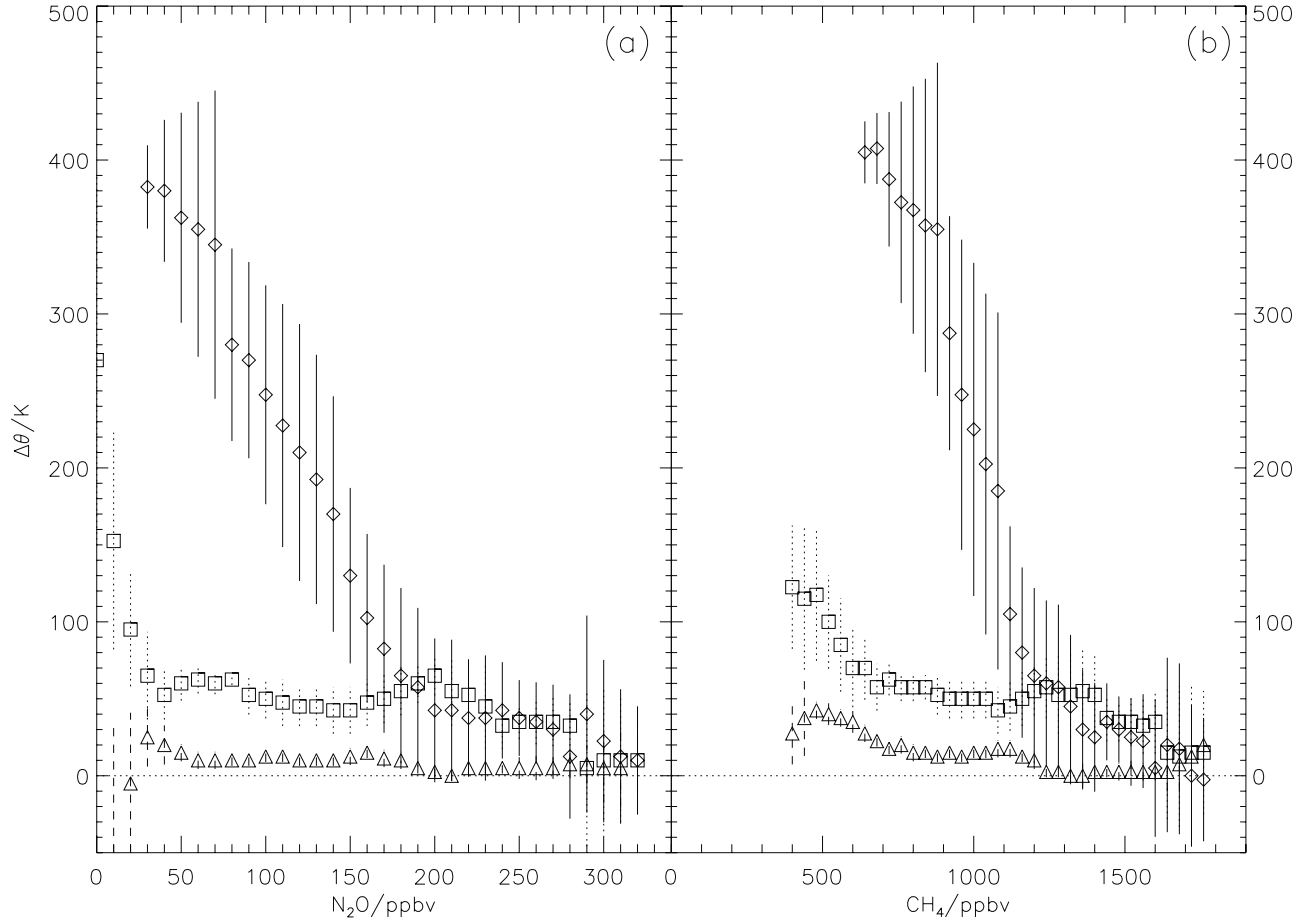

Figure 8. Differences between profiles for (a) N_2O and (b) CH_4, indicating descent (assuming no mixing). Vertical bars indicate $\pm 1\sigma$ uncertainties, which are calculated as the quadrature sum of individual profile uncertainties. Legend: START to 26 November 1999 fall vortex (diamonds/solid line), 26 November 1999 fall vortex to 27 January 2000 BONBON (squares/dotted line), 27 January 2000 BONBON to 5 March 2000 LACE (triangles/dashed line), zero line (dotted horizontal line).

10 K. Between 27 January and 5 March, $\Delta\theta$ was smaller still, only 10 ± 6 K over the same ranges. The differences between the START profile and the 5 March LACE profile (not shown), as an indication of the total descent during 1999/2000, ranged from 501 ± 21 K at 30 ppbv N_2O and 640 ppbv CH_4 to 49 ± 23 K above 200 ppbv N_2O and 1280 ppbv CH_4.

[50] It is important to emphasize that these results probably represent underestimates of the amount of descent, because the effects of mixing have not been accounted for. "Mixing" here indicates the process of vortex homogenization, incorporating air that has either become entrained from midlatitudes, or undergone differential diabatic descent within the vortex. In either situation, adjacent air masses will have undergone different amounts of descent, and tend to mix along θ surfaces. Both of these processes can be active during vortex formation in the fall, and can substantially alter tracer:tracer as well as tracer:θ relationships [*Plumb et al.*, 2000]. The general effect is to reduce the apparent descent [*Abrams et al.*, 1996b; *Müller et al.*, 1996]. However, once the vortex has become isolated from the rest of the stratosphere, which is typically complete by late fall, the assumption of no mixing is a fairly good one. For instance, in the study by *Ray et al.* [2002], which explicitly modeled mixing as a result of differential diabatic descent in the early fall, only small changes (<20 K) in the calculated descent between the 19 November 1999 and 5 March 2000 LACE measurements were seen relative to the simple case where mixing was ignored.

[51] Descent rates are shown in Figures 9a–9e, as well as in Table 2. Rates are shown for all profile pairs shown in Figure 8, with the exception of the START to 26 November difference, since the effective 1999 date of the START profile was not known. Rates for several unified N_2O profile pairs are also shown. Although the unified N_2O-based rates display generally higher error bars than those based on the balloon data, the latter were included because their higher time density enabled a more detailed temporal reconstruction of the descent rates. There is a general decrease in the descent rate with time for all N_2O isopleths shown, ranging from between 0.56 ± 0.18 and 1.05 ± 0.21 K/day in the earliest time interval (26 November to 27 January), to between -0.17 ± 0.37 and 0.33 ± 0.47 K/day in the latest interval (26 February to 12 March). This is entirely expected, and is a reflection of increasing solar radiation slowly reducing the net radiative cooling as winter passes into spring. There is also a general decrease in the rate with increasing N_2O isopleth:

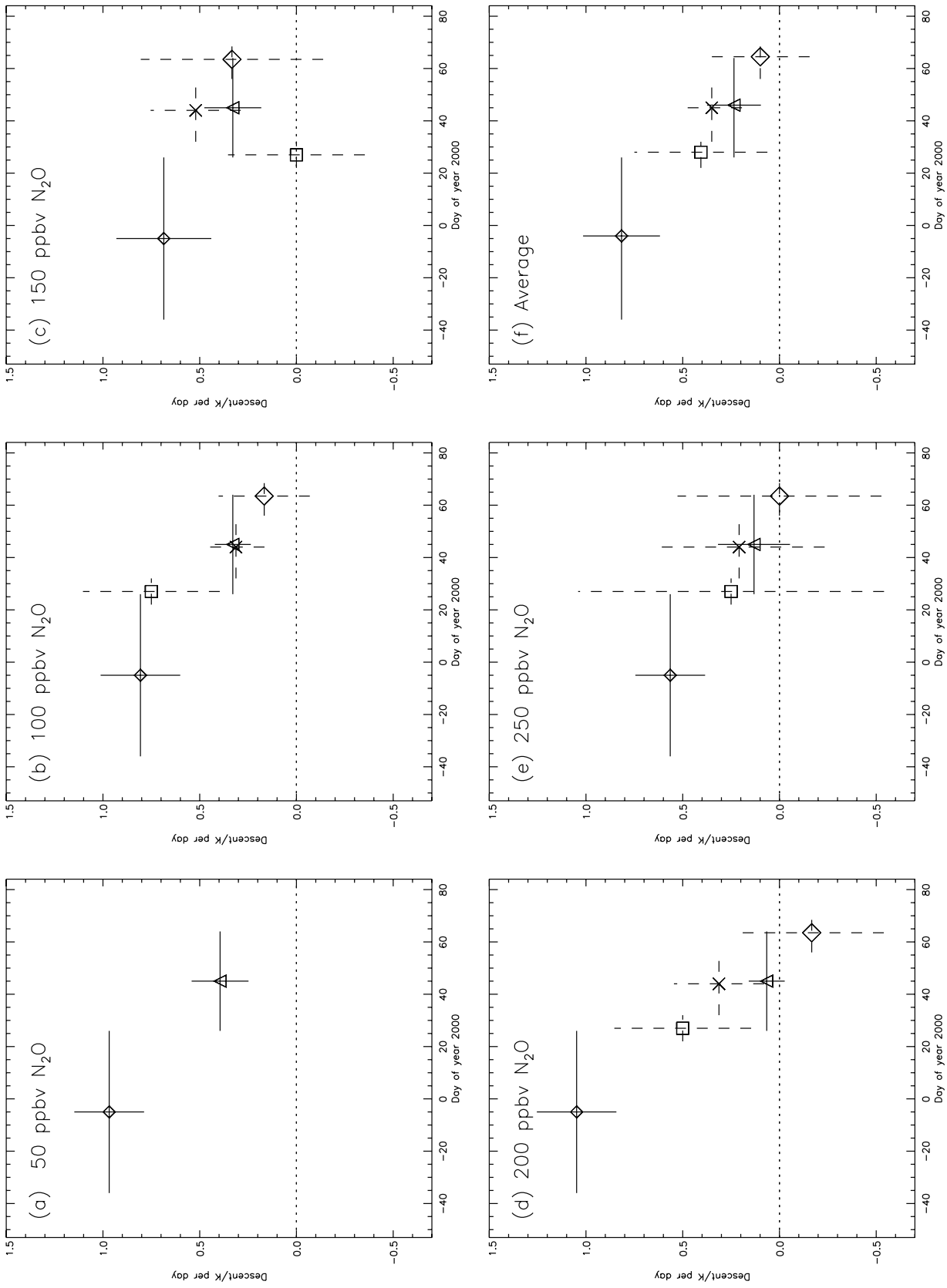
(a) 50 ppbv N_2O
(b) 100 ppbv N_2O
(c) 150 ppbv N_2O
(d) 200 ppbv N_2O
(e) 250 ppbv N_2O
(f) Average
Descent/K per day
Day of year 2000

Table 2. Calculated Descent Rates (K/day) for the 1999/2000 Winter[a]

	N_2O Isopleth, ppbv					
Range of Dates	50	100	150	200	250	Average
			Balloon Measurements			
26 Nov. to 27 Jan.	0.97 ± 0.18	0.81 ± 0.21	0.69 ± 0.25	1.05 ± 0.21	0.56 ± 0.18	0.82 ± 0.20
27 Jan. to 5 March	0.39 ± 0.15	0.33 ± 0.09	0.33 ± 0.15	0.07 ± 0.09	0.13 ± 0.19	0.24 ± 0.14
			Unified N_2O Measurements			
23 Jan. to 2 Feb.	n/a	0.75 ± 0.35	0.00 ± 0.35	0.50 ± 0.35	0.25 ± 0.79	0.41 ± 0.34
2 to 26 Feb.	n/a	0.31 ± 0.15	0.52 ± 0.23	0.31 ± 0.23	0.21 ± 0.44	0.35 ± 0.16
26 Feb. to 12 March	n/a	0.17 ± 0.24	0.33 ± 0.47	−0.17 ± 0.37	0.00 ± 0.53	0.10 ± 0.25
			Winter Average			
26 Nov. to 5 March	0.75 ± 0.10	0.63 ± 0.13	0.55 ± 0.16	0.68 ± 0.13	0.40 ± 0.11	0.61 ± 0.13

[a] Uncertainties are 1σ.

e.g., for the time interval 27 January to 5 March, the rate decreases from 0.39 ± 0.15 K/day at 50 ppbv to 0.13 ± 0.19 K/day at 250 ppbv. This N_2O trend reflects the greater radiative cooling at higher altitudes, while the much lower descent by 250 ppbv is indicative of the increased mixing near the tropopause. However, a notable exception is the 200 ppbv isopleth, which has the highest descent rate in the earliest interval.

[52] Weighted average descent rates across N_2O isopleths for each time interval are also shown in Figure 9f, as well as in Table 2, decreasing from 0.82 ± 0.20 K/day between 26 November and 27 January to 0.10 ± 0.25 26 February to 12 March. Finally, a winter average descent rate (between 26 November and 5 March; results for 26 November to 12 March are very similar) is shown in Table 2 for each N_2O isopleth, as well as a grand average. A decrease from 0.75 ± 0.10 K/day at 50 ppbv to 0.40 ± 0.11 K/day at 250 ppbv is observed, with the average winter 1999/2000 descent rate across 50–250 ppbv N_2O at 0.61 ± 0.13 K/day.

3.8. Comparison With Other Studies

[53] Descent rates have been reported for several previous winters relative to θ [*Schoeberl et al.*, 1992; *Rosenfield et al.*, 1994; *Strahan et al.*, 1994; *Lucic et al.*, 1999], altitude (*z*) [*Schoeberl et al.*, 1992; *Rosenfield et al.*, 1994; *Traub et al.*, 1995; *Abrams et al.*, 1996a], and/or tracer isopleth [*Bauer et al.*, 1994; *Müller et al.*, 1996; *Hartmann et al.*, 1997], and over a wide range of time periods. In order to compare our results with previously reported values, we have related values found in the literature to N_2O isopleths, as summarized in Table 3. The methods used for each study are explained in the footnotes to Table 3.

[54] Over the period represented by these studies (1988–1996), the Arctic winter stratosphere exhibited substantial interannual variations in temperature fields [e.g., *National Oceanic and Atmospheric Administration* (*NOAA*), 2000], planetary wave activity [*Waugh et al.*, 1999], and ozone loss [*Rex et al.*, 2002]. We have found, however, that for descent rates reported relative to θ, the agreement is generally consistent with our 1999/2000 rates (see Table 2), with two exceptions.

[55] *Rosenfield et al.* [1994], who simulated both the 1988/1989 and 1991/1992 winters, reported average rates for 22 January to 21 March (0.60–0.95 K/day) which were significantly higher than the similar time period 27 January to 5 March in our study (0.07 ± 0.09 to 0.39 ± 0.15 K/day). While the *Rosenfield et al.* [1994] results were similar in magnitude to the 1991/1992 study of *Lucic et al.* [1999] (0.55–0.9 K/day), that study began earlier in the year (7 December), where larger descent rates would be expected. The only other 1988/1989 study included here which calculated descent rates after 1 January was that of *Schoeberl et al.* [1992], and those descent rates were much lower (0.09 ± 0.16 to 0.36 ± 0.05 K/day).

[56] *Bauer et al.* [1994] reported observation-based descent rates from 31 October 1991 to 18 January 1992 of 2.7–3.4 K/day at 50–100 ppbv N_2O, far higher than those calculated for the similar period 26 November to 27 January in our study (0.81 ± 0.21 to 0.97 ± 0.18 K/day). The difference may be partly due to the earlier starting time of the calculation; *Strahan et al.* [1994] reported a model descent rate for October 1991 of 1.2 K/day at 250 ppbv N_2O; although not reported in the study, the rate at 50–100 ppbv would probably be much larger, consistent with the pattern of larger rates on lower N_2O isopleths. However, *Rosenfield et al.* [1994], who began their simulation on 1 November, almost coincident with the first *Bauer et al.* [1994] profile, reported substantially smaller rates though 22 January (1.02–1.20 K/day at 50–100 ppbv N2O), consistent with our results. It is possible that the *Bauer et al.* [1994] study, which utilized data from one launch location, sampled anomalously large local descent, which was not observable in the vortex average study of *Rosenfield et al.* [1994].

[57] It was hoped that by examining studies that reported descent rates in terms of both θ and *z*, a simple correspond-

Figure 9. (opposite) Descent rates (K/day) on different N_2O isopleths for pairs of profiles on five N_2O isopleths in panels (a)–(e), and average descent rates in panel (f). Horizontal bars indicate time differences, and vertical bars indicate ±1σ uncertainties. Legend: 26 November 1999 fall vortex to 27 January 2000 BONBON (diamond/solid line), 27 January 2000 BONBON to 5 March 2000 LACE (triangle/solid line), 20 January to 2 February 2000 unified N_2O (square/dashed line), 2–26 February 2000 unified N_2O (X/dashed line), 26 February to 12 March 2000 unified N_2O (diamond/dashed line), zero line (dotted horizontal line).

Table 3. Descent Rate Comparison With Other Studies[a]

Reference	Year(s)	Time Period	θ, K	*Z*, km	N_2O, ppbv	Descent Rate, K/day	Descent Rate, m/day
			Observations				
Schoeberl et al. [1992]	1988/1999	3 Jan. to 10 Feb.	450[b]	20[b]	110[c]	0.36 ± 0.05[b]	98 ± 20[b]
			420[b]	18[b]	160[c]	0.27 ± 0.11[b]	69 ± 33[b]
			390[b]	16.5[b]	210[c]	0.09 ± 0.16[b]	12 ± 35[b]
Bauer et al. [1994]	1991/1992	31 Oct. to 18 Jan.	510[d]	21.0[d]	50	3.4[e]	97[e]
			445[d]	18.4[d]	100	2.7[e]	113[e]
Strahan et al. [1994]	1991/1992	Dec. to Feb.	410	n/a	160–230[f]	0.5	n/a
			470	n/a	100–140[f]	0.7	n/a
Traub et al. [1995]	1991/1992	Jan. to Feb.	n/a	18	120[g]	n/a	51 ± 8
Abrams et al. [1996a]	1992/1993	Oct./Nov.–Apr.	n/a	30	55[h]	n/a	62
			n/a	24	120[h]	n/a	39
			n/a	20	180[h]	n/a	24
Müller et al. [1996]	1991/1992 to 1995/1996	Nov./Dec. to Apr.	420[i]	n/a	150[g]	0.5–0.6[h]	40[h]
Hartmann et al. [1997]	1994/1995	7 Oct. to 22 Mar.	n/a	20[d]	100[i]	n/a	66
			n/a	19[d]	120[i]	n/a	41
			n/a	18[d]	170[i]	n/a	15
			n/a	16[d]	250[i]	n/a	11
			Models				
Schoeberl et al. [1992]	1988/1999	3 Jan. to 10 Feb.	450[b]	n/a	110[c]	0.31 ± 0.12[b]	n/a
			360[b]	n/a	240[c]	0.24 ± 0.06[b]	n/a
Rosenfield et al. [1994]	1988/1999 and 1991/1992	1 Nov. to 22 Jan.[l]	500[d,m]	20.2[d,m]	50[c]	1.20[e]	34[e]
		1 Nov. to 22 Jan.[l]	465[d,m]	n/a	100[c]	1.02[e]	n/a
		1 Nov. to 22 Jan.[l]	430[d,m]	17.1[d,m]	140–150[c]	0.84[e]	35[e]
		1 Nov. to 22 Jan.[l]	390[d,m]	15.4[d,m]	200–210[c]	0.72[e]	31[e]
		22 Jan.[l] to 21 Mar.	445[d,m]	15.5[d,m]	50[c]	0.95[e]	81[e]
		22 Jan.[l] to 21 Mar.	420[d,m]	n/a	100[c]	0.78[e]	n/a
		22 Jan.[l] to 21 Mar.	395[d,m]	13.6[d,m]	140–150[c]	0.60[e]	60[e]
		22 Jan.[l] to 21 Mar.	355[d,m]	12.2[d,m]	200–210[c]	0.60[e]	55[e]
Strahan et al. [1994]	n/a	Oct.	460[n]	n/a	250[o]	1.2[n]	n/a
		Dec.	415[n]	n/a	250[o]	0.75[n]	n/a
		Dec.	470[n]	n/a	150[o]	0.9[n]	n/a
		Jan.	450[n]	n/a	150[o]	0.8[n]	n/a
		Feb.	435[n]	n/a	150[o]	0.6[n]	n/a
		Mar.	435[n]	n/a	150[o]	0.2[n]	n/a
Lucic et al. [1999]	1991/1992	7 Dec. to 15 Mar.	475	n/a	70[o]	0.65–0.9	n/a
			400	n/a	250[o]	0.55[p]	n/a

[a] Uncertainties are 1s. Potential temperature is denoted by q; altitude, by z. Numbers without footnotes indicate they were taken directly from the text or table in the reference.
[b] Estimated from *Schoeberl et al.* [1992, Figure 4].
[c] Estimated from N_2O:q average profile for 3 January to 10 February 1989 from *Schoeberl et al.* [1992, Figure 4].
[d] Value of q (or z) of ending profile.
[e] Calculated from q (or z) differences.
[f] Estimated from observed N_2O:q from *Strahan et al.* [1994, Figure 3].
[g] Estimated from N_2O:z profile average for January to February 1989 from *Loewenstein et al.* [1990, Figure 4].
[h] Estimated from N_2O:q profile from *Abrams et al.* [1996a, Figure 2].
[i] Estimated from N_2O:CH_4 correlation fit (this paper).
[j] Estimated from difference in q (or z) divided by 150 days.
[k] Estimated from N_2O:CCl_2F_2 correlation from *Hartmann et al.* [1997, Figure 5].
[l] The 22nd of January corresponds to middle date of flights reported by *Schoeberl et al.* [1992].
[m] Estimated from *Rosenfield et al.* [1994, Figures 4 and 5].
[n] Estimated from *Strahan et al.* [1994, Figure 5].
[o] Estimated from SKYHI N_2O:q profiles from *Strahan et al.* [1994, Figure 2].
[p] Estimated from *Lucic et al.* [1999, Figure 6].

ence could be derived between the two sets of rates. However, the data showed little or no relationship between the two coordinate systems; for instance, *Rosenfield et al.* [1994] reported a substantial increase in the *z*-based descent rates after 22 January, whereas the θ-based rates in the same study decreased markedly. Another example is *Bauer et al.* [1994], whose *z*-based rates, while on the high end of the range reported by other studies, did not stand out nearly as much as the θ-based rates discussed earlier (see Table 3). Thus the relationship between θ and *z* appears complex, and we did not attempt to make any comparison between studies that reported descent rates in terms of *z* and the θ-based 1999/2000 descent rates.

3.9. Model Comparisons

[58] Figure 10 shows the comparison between the REPROBUS model and fits of the observational data. The agreement differed considerably from N_2O to CH_4, with each tracer exhibiting better agreement on some isopleths and worse agreement on others. In terms of absolute differences, the N_2O model data agreed most favorably with the observational fits from 150–250 ppbv, while the CH_4 data

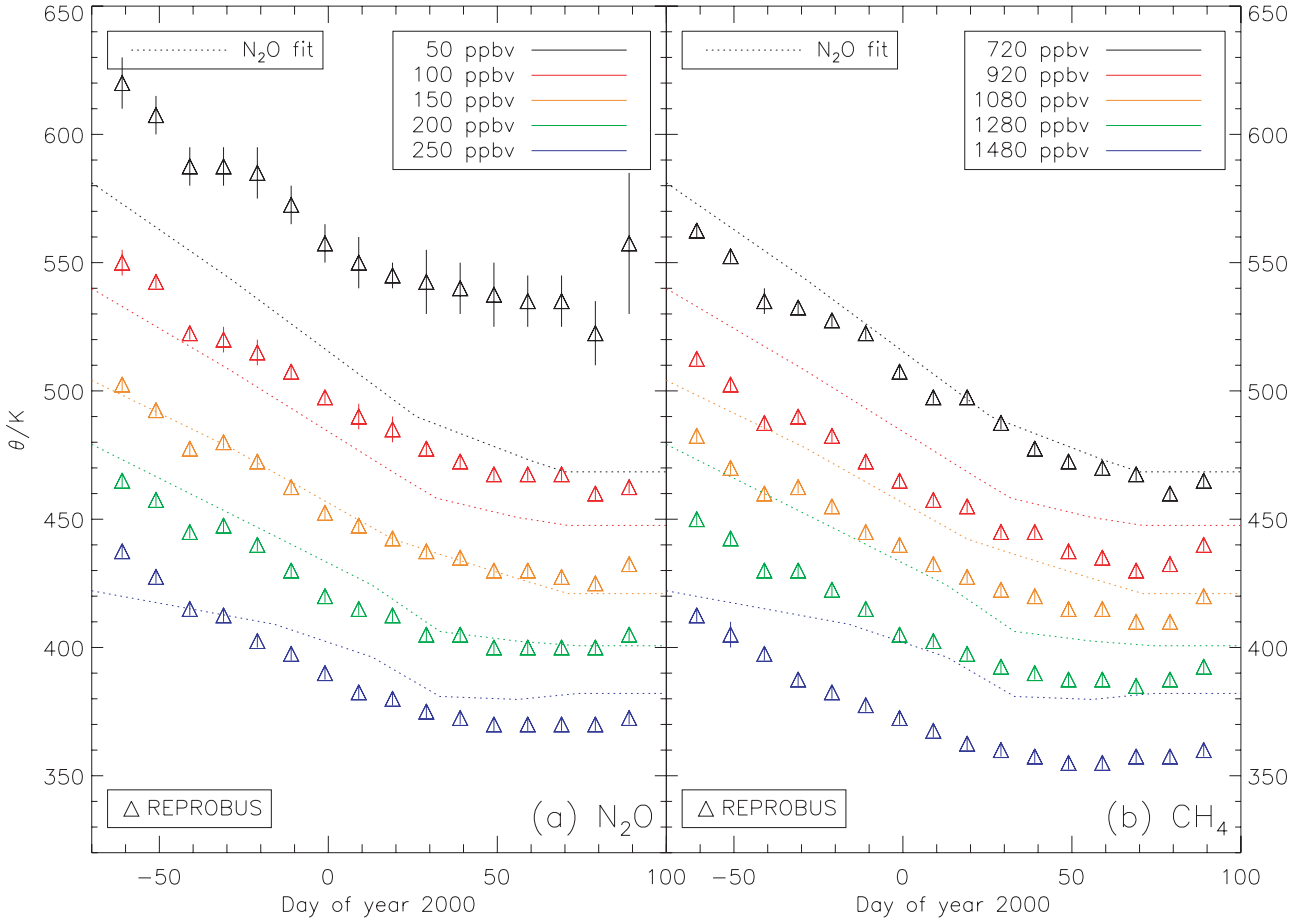

Figure 10. Comparison of fits of observed data with the REPROBUS model for (a) N_2O and (b) CH_4. Colors denote different isopleths following the same scheme as in Figure 6. Symbols indicate 1-day snapshots, with vertical bars indicating ±1σ uncertainties. Dotted lines are the N_2O fits from Figure 6.

agreed quite well for the 720 ppbv isopleth (equivalent to 50 ppbv N_2O), but had worse agreement for all other isopleths. Most of the differences observed may be due to poor model tracer initializations and/or inadequate model tracer photochemistry. However, while the differences between model and observation may be considerable for several isopleths, they did not change significantly with time (with the exception of the 50 ppbv N_2O and 1480 ppbv CH_4 isopleths, whose model observation differences increased markedly with time). This relative agreement indicates that the model-derived descent rates were, in fact, fairly accurate throughout the winter. The disagreement at 50 ppbv N_2O may indicate that descent was not strong enough in the model at these altitude levels, while the disagreement at 1480 ppbv CH_4 was probably due to the close proximity to the bottom of the vortex, which is typically located near 400 K [e.g., *Manney et al.*, 1994].

[59] A comparison of the SLIMCAT N_2O results and fits of the observational data is shown in Figure 11. Offsets between model and observation were of the same magnitude (~20 K) as the REPROBUS differences for the 100–250 ppbv isopleths, and the 50 ppbv isopleth agreed much better with the observed data than did the 50 ppbv N_2O REPROBUS isopleth. There was a slight change in the offsets between 100 and 200 ppbv around day 27, resulting in better agreement between model and observation, while the 250 ppbv isopleth offset increased slightly over time. The 50 ppbv isopleth, despite its larger error bars, appeared to track the observed data best, with the exception of days 37 and 87, where error bars were much higher; these increases were associated with a more distorted vortex, resulting in a significantly wider range of VMRs sampled in the 70°–80°N EqL region. Despite these θ offsets, the good agreement in slopes between the SLIMCAT results and the observations indicated that the descent rates calculated were very similar to those derived from our study.

4. Summary

[60] The descent of the 1999/2000 Arctic vortex has been quantified using N_2O and CH_4 tracer measurements from a number of instruments. Coverage spanned the last stages of vortex formation in late November 1999 through vortex breakup in mid-March 2000, with two large gaps (17 December to 13 January and 4–25 February). Changes in θ were determined on five N_2O and CH_4 isopleths, and descent rates were calculated on each N_2O isopleth for several time intervals throughout the fall and winter. From 26 November to 5 March the vortex descended 65 ± 12 K when averaged over 40–280 ppbv N_2O and 680–1600

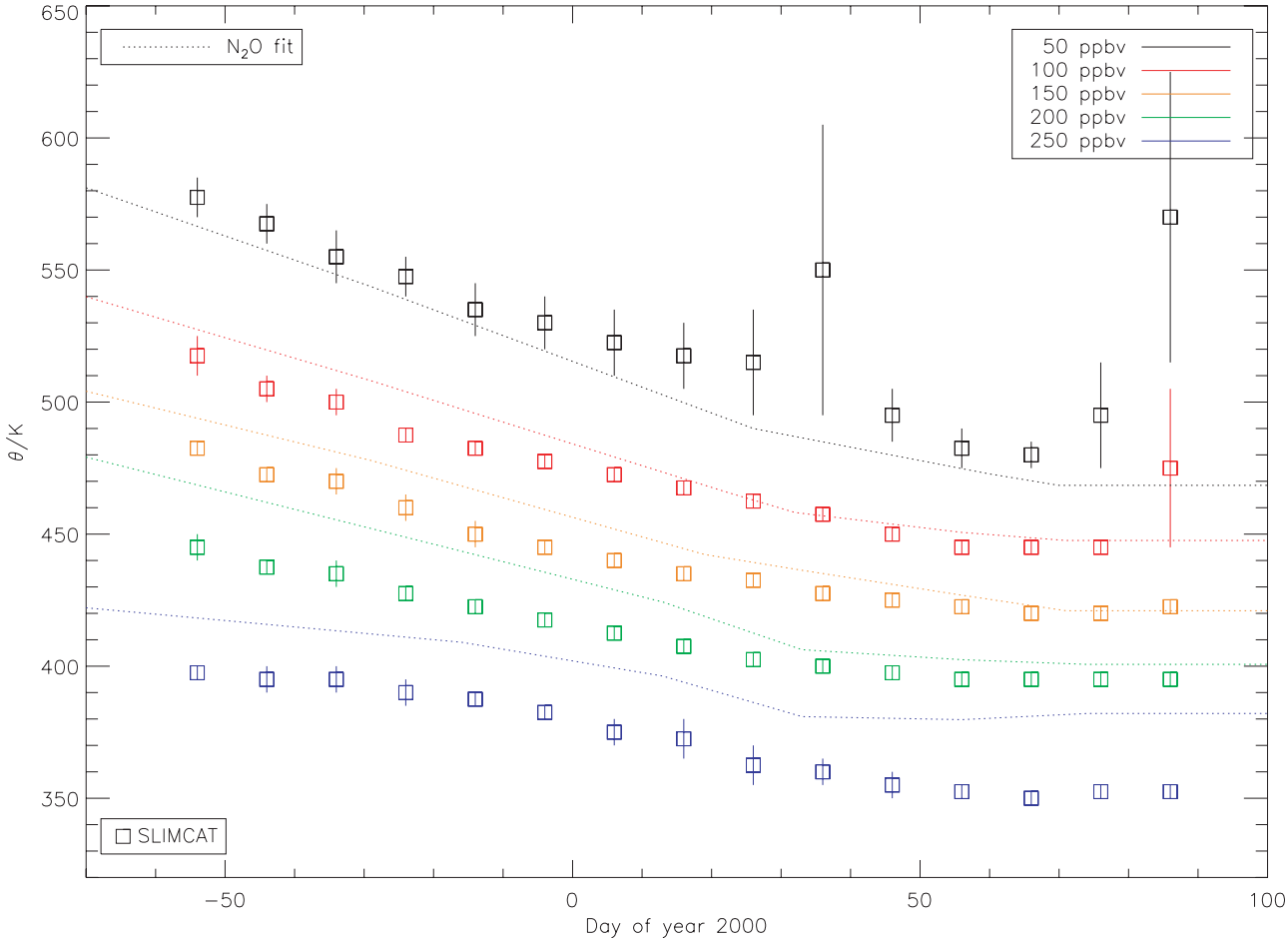

Figure 11. Comparison of fits of observed data with the SLIMCAT model for N_2O. Colors denote different isopleths following the same scheme as in Figure 6. Symbols indicate 10-day averages, with vertical bars indicating ±1σ uncertainties. Dotted lines are the N_2O fits from Figure 6.

ppbv CH_4. The maximum descent rates occurred in the late fall/early winter phase: between 26 November and 27 January, the calculated rate was 0.82 ± 0.20 K/day averaged over 50–250 ppbv N_2O. By late winter (26 February to 12 March), the average rate had decreased to 0.10 ± 0.25 K/day. Descent rates also decreased with increasing N_2O isopleth; for instance, the winter average (26 November to 5 March) descent rate varied from 0.75 ± 0.10 K/day at 50 ppbv to 0.40 ± 0.11 K/day at 250 ppbv. The winter average rate over 50–250 ppbv N_2O was 0.61 ± 0.13 K/day.

[61] Larger variability in θ on tracer isopleths in late fall versus winter indicated that the vortex was much less homogenous in the late fall. The degree of inhomogeneity, derived from several instruments (LACE, MkIV, SLS, and ASUR), was 19–23 K over the range 110–200 ppbv N_2O and 960–1200 ppbv CH_4. This inhomogeneity decreased significantly in the March data sets; the unified N_2O variability averaged only 7.4 K at 200 ppbv N_2O. Because of the vortex inhomogeneity in late fall, an average fall vortex profile was constructed from the 19 November LACE and 3 December MkIV measurements, which encompassed the observed variability of all the fall measurements. This profile, referred to as the 26 November 1999 vortex average, was used in subsequent calculations of vortex descent.

[62] A comparison of high-latitude, extravortex profiles measured in different years and seasons, while revealing significant VMR differences on a given θ level, also showed that extravortex profiles were more similar to each other than to the late fall profiles. Therefore, the median profile, an average extravortex profile measured by ATMOS in November 1994, was chosen as the vortex starting profile for 1999/2000 (denoted "START") and was used to estimate the amount of descent prior to the first vortex measurements in November and December. The difference between the START profile and the 26 November average profile showed significant descent prior to the first profiles measured in fall 1999/2000, up to 397 ± 15 K at the lowest N_2O and CH_4 levels (30 ppbv N_2O and 640 ppbv CH_4), and falling to 28 ± 13 K for N_2O larger than 200 ppbv and CH_4 larger than 1280 ppbv. Such early descent has been inferred for prior years in the Arctic, e.g., 1988/1989 and 1991/1992 [*Rosenfield et al.*, 1994], 1993/1994 [*Abrams et al.*, 1996a] and 1994/1995 [*Michelsen et al.*, 1998b]. While these differences did not include the effects of mixing, as first-order approximations they indicated that a great deal of descent had occurred prior to the late fall vortex measurements.

[63] Descent rates from previous θ-based studies corroborate the results of our study very well across a wide range

of time periods and N_2O isopleths, with the exception of one observational study [*Bauer et al.*, 1994] and the late winter time period of one model study [*Rosenfield et al.*, 1994]. Because it has been shown, both with our own results and those of prior studies, that descent rates increase substantially with decreasing N_2O or increasing altitude, it is more meaningful and useful to calculate rates for several tracer isopleths (as we have done), θ levels, or z levels, than to report a single number. Likewise, because of the large change in descent rates observed throughout the fall and winter, a single, season average descent rate is not as informative as rates reported for several selected times.

[64] Both the REPROBUS and SLIMCAT models calculated descent rates that agreed quite favorably with observations. Although both models showed disagreements with observations of up to $\sim$20 K (except for the 50 ppbv N_2O isopleth of REPROBUS), the causes were somewhat different for each model. For REPROBUS, the quality of the tracer initializations directly affected the agreement, as there was no ''spin-up'' period in the model. For SLIMCAT, where tracer distributions were initiated in 1991, the differences with observation were due almost exclusively to model chemistry and transport, which over the eight year run time of the model should be regarded as very good. Given the different approaches employed by the two models for deriving these rates (direct use of the vertical wind field component for REPROBUS versus a radiative model for SLIMCAT), the success of both models in reproducing the observed descent *via* trace gas measurements should be highlighted.

[65] **Acknowledgments.** We thank James J. Margitan (Jet Propulsion Laboratory) for providing potential temperature data from his ozone instrument on the 19 November 1999 balloon flight, Paul A. Newman and Leslie R. Lait (NASA Goddard) for providing Nash algorithm analysis of PV data for 1999/2000, Ingeborg Levin (Institut für Umweltphysik, Heidelberg, Germany) for performing the CH_4 analysis for the BONBON flight of 30 November 1991, F. William Irion and Michael R. Gunson (Jet Propulsion Laboratory) for producing the ATMOS version 3 data sets used in this paper, and Hope A. Michelsen (Sandia National Laboratories) for providing averaged extravortex ATMOS data from 1993 and 1994. We are indebted to Susan E. Strahan (NASA Goddard) and Rolf Müller (Forschungszentrum Jülich) for helpful discussions and to Gloria L. Manney (Jet Propulsion Laboratory/New Mexico Highlands University), Hope A. Michelsen, Leonhard Pfister (NASA Ames), and Henry (Rennie) Selkirk (NASA Ames) for commentary on the manuscript. Thanks go to Jeff Grose (NASA Ames) for his expertise in all aspects of the Argus instrument operations, the crews and pilots of the ER-2 and DC-8 aircraft (NASA Dryden), the Centre National d'Études Spatiales (CNES), and the National Scientific Balloon Facility (NSBF) teams for flight operations during the difficult conditions of the Arctic winter. We thank Michael Kurylo and Phil DeCola (NASA Headquarters) for funding SOLVE investigators and the European Commission for funding THESEO 2000 investigators. We thank the Forschungszentrum Jülich for funding the BONBON balloon flight on 1 March 2000. M. Chipperfield and B.-M. Sinnhuber are grateful to the UK Natural Environment Research Council's Upper Troposphere/Lower Stratosphere (UTLS) Programme, which provided funding for their work. J. Greenblatt is grateful for funds provided by the National Research Council, which made his research at NASA Ames possible.

References

Abrams, M. C., et al., Trace gas transport in the Arctic vortex inferred from ATMOS ATLAS-2 observations during April 1993, *Geophys. Res. Lett.*, *23*, 2345–2348, 1996a.

Abrams, M. C., et al., ATMOS ATLAS-3 observations of long-lived tracers and descent in the Antarctic vortex in November 1994, *Geophys. Res. Lett.*, *23*, 2341–2344, 1996b.

Allen, D. R., J. L. Stanford, N. Nakamura, M. A. López-Valverde, M. López-Puertas, F. W. Taylor, and J. J. Remedios, Antarctic polar descent and planetary wave activity observed in ISAMS CO from April to July 1992, *Geophys. Res. Lett.*, *27*, 665–668, 2000.

Bacmeister, J. T., M. R. Schoeberl, M. E. Summers, J. R. Rosenfield, and X. Zhu, Descent of long-lived trace gases in the winter polar vortex, *J. Geophys. Res.*, *100*, 11,669–11,684, 1995.

Bauer, R., A. Engel, H. Franken, E. Klein, G. Kulessa, C. Schiller, U. Schmidt, R. Borchers, and J. Lee, Monitoring the vertical structure of the Arctic polar vortex over northern Scandinavia during EASOE: Regular N_2O profile observations, *Geophys. Res. Lett.*, *21*, 1211–1214, 1994.

Brasseur, G., and S. Solomon, *Aeronomy of the Middle Atmosphere*, 2nd ed., 452 pp., D. Reidel, Norwell, Mass., 1995.

Butchart, N., and E. E. Remsberg, The area of the stratospheric polar vortex as a diagnostic for tracer transport on an isentropic surface, *J. Atmos. Sci.*, *43*, 1319–1339, 1986.

Chang, A. Y., et al., A comparison of measurements from ATMOS and instruments aboard the ER-2 aircraft: Tracers of atmospheric transport, *Geophys. Res. Lett.*, *23*, 2389–2392, 1996.

Chipperfield, M. P., Multiannual simulations with a three dimensional chemical transport model, *J. Geophys. Res.*, *104*, 1781–1805, 1999.

Crewell, S., D. Cheng, R. L. de Zafra, and C. Trimble, Millimeter wave spectroscopic measurements over the South Pole, 1. A study of stratospheric dynamics using N_2O observations, *J. Geophys. Res.*, *100*, 20,839–20,844, 1995.

Elkins, J. W., et al., Airborne chromatograph for in situ measurements of long-lived species in the upper troposphere and lower stratosphere, *Geophys. Res. Lett.*, *23*, 347–350, 1996.

Eluszkiewicz, J., R. A. Plumb, and N. Nakamura, Dynamics of wintertime stratospheric transport in the Geophysical Fluid Dynamics Laboratory SKYHI general circulation model, *J. Geophys. Res.*, *100*, 20,883–20,900, 1995.

Emmons, L. K., J. M. Reeves, D. T. Shindell, and R. L. de Zafra, N_2O as an indicator of Arctic vortex dynamics: Correlations with O_3 over Thule, Greenland in February and March, 1992, *Geophys. Res. Lett.*, *21*, 1275–1278, 1994.

Fairlie, T. D., R. B. Pierce, J. A. Al-Saadi, W. L. Grose, J. M. Russell III, M. H. Proffitt, and C. R. Webster, The contribution of mixing in Lagrangian photochemical predictions of polar ozone loss over the Arctic in summer 1997, *J. Geophys. Res.*, *104*, 26,597–26,609, 1999.

Fisher, M., A. O'Neill, and R. Sutton, Rapid descent of mesospheric air into the stratospheric polar vortex, *Geophys. Res. Lett.*, *20*, 1267–1270, 1993.

Greenblatt, J. B., et al., Defining the polar vortex edge from an N_2O: potential temperature correlation, *J. Geophys. Res.*, *107*, 10.1029/2001JD000575, in press, 2002.

Gunson, M. R., et al., The Atmospheric Trace Molecule Spectroscopy (ATMOS) experiment: Deployment on the ATLAS Space Shuttle missions, *Geophys. Res. Lett.*, *23*, 2333–2336, 1996.

Hartmann, J.-M., J.-M. Kochel, S. Payan, C. Camy-Péyret, and A. Engel, CCl_2F_2 mixing ratio profiles in the 1995 late winter Arctic vortex from balloon-borne spectra, *Geophys. Res. Lett.*, *24*, 2367–2370, 1997.

Herman, R. L., et al., Tropical entrainment time scales inferred from stratospheric N_2O and CH_4 observations, *Geophys. Res. Lett.*, *25*, 2781–2784, 1998.

Hurst, D. F., et al., Construction of unified, high-resolution nitrous oxide data set for ER-2 flights during SOLVE, *J. Geophys. Res.*, *107*, 8271, doi:10.1029/2001JD000417, 2002.

Intergovernmental Panel on Climate Change (IPCC), *Climate Change 1995: The Science of Climate Change*, edited by J. T. Houghton et al., Cambridge Univ. Press, New York, 1996.

Jost, H., and M. Loewenstein, Argus: A lightweight TDL instrument to measure stratospheric tracers, in *Application of Tunable Diode and Other Infrared Sources for Atmospheric Studies and Industrial Process Monitoring II*, Int. Soc. for Opt. Eng. Bellingham, Wash., 1999.

Jost, H., M. Loewenstein, L. Pfister, J. J. Margitan, A. Y. Chang, R. J. Salawitch, and H. A. Michelsen, Laminae in the tropical middle stratosphere: Origin and age estimation, *Geophys. Res. Lett.*, *25*, 4337–4340, 1998.

Kawamoto, N., and M. Shiotani, Interannual variability of the vertical descent rate in the Antarctic polar vortex, *J. Geophys. Res.*, *105*, 11,935–11,946, 2000.

Lait, L. R., An alternative form for potential vorticity, *J. Atmos. Sci.*, *51*, 1754–1759, 1994.

Lefèvre, F., G. P. Brasseur, I. Folkins, A. K. Smith, and P. Simon, Chemistry of the 1991–1992 stratospheric winter: Three-dimensional model simulations, *J. Geophys. Res.*, *99*, 8183–8195, 1994.

Lefèvre, F., F. Figarol, K. S. Carslaw, and T. Peter, The 1997 Arctic ozone depletion quantified from three-dimensional model simulations, *Geophys. Res. Lett.*, *25*, 2425–2428, 1998.

Loewenstein, M., J. R. Podolske, K. R. Chan, and S. E. Strahan, Nitrous

oxide as a dynamical tracer in the 1987 Airborne Antarctic Ozone Experiment, *J. Geophys. Res.*, *94*, 11,589–11,598, 1989.

Loewenstein, M., J. R. Podolske, K. R. Chan, and S. E. Strahan, N_2O as a dynamical tracer in the Arctic vortex, *Geophys. Res. Lett.*, *17*, 477–480, 1990.

Lucic, D., N. R. P. Harris, J. A. Pyle, and R. L. Jones, A technique for estimating polar ozone loss: Results for the northern 1991/92 winter using EASOE data, *J. Atmos. Chem.*, *34*, 365–383, 1999.

Manney, G. L., and J. L. Sabutis, Development of the polar vortex in the 1999–2000 Arctic winter stratosphere, *Geophys. Res. Lett.*, *27*, 2589–2592, 2000.

Manney, G. L., R. W. Zurek, A. O'Neill, and R. Swinbank, On the motion of air through the stratospheric polar vortex, *J. Atmos. Sci.*, *51*, 2973–2994, 1994.

Manney, G. L., et al., Lagrangian transport calculations using UARS data, 1, Passive tracers, *J. Atmos. Sci.*, *52*, 3049–3068, 1995.

Manney, G. L., H. A. Michelsen, M. L. Santee, M. R. Gunson, F. W. Irion, A. E. Roche, and N. J. Livesey, Polar vortex dynamics during spring and fall diagnosed using trace gas observations from the Atmospheric Trace Molecule Spectroscopy instrument, *J. Geophys. Res.*, *104*, 18,841–18,866, 1999.

Manney, G. L., H. A. Michelsen, F. W. Irion, G. C. Toon, M. R. Gunson, and A. E. Roche, Lamination and polar vortex development in the fall from ATMOS long-lived trace gases observed during November 1994, *J. Geophys. Res.*, *105*, 29,023–29,038, 2000.

McIntyre, M. E., Atmospheric dynamics: Some fundamentals, with observational implications, in *The Use of EOS for Studies of Atmospheric Physics*, edited by J. C. Gille and G. Visconti, pp. 313–386, North-Holland, New York, 1992.

Michelsen, H. A., G. L. Manney, M. R. Gunson, C. P. Rinsland, and R. Zander, Correlations of stratospheric abundances of CH_4 and N_2O derived from ATMOS measurements, *Geophys. Res. Lett.*, *25*, 2777–2780, 1998a.

Michelsen, H. A., G. L. Manney, M. R. Gunson, and R. Zander, Correlations of stratospheric abundances of NO_y, O_3, N_2O and CH_4 derived from ATMOS measurements, *J. Geophys. Res.*, *103*, 28,347–28,359, 1998b.

Michelsen, H. A., et al., Intercomparison of ATMOS, SAGE II, and ER-2 observations in Arctic vortex and extravortex air masses during spring 1993, *Geophys. Res. Lett.*, *26*, 291–294, 1999.

Moore, F. L., et al., Balloonborne in situ gas chromatography for measurements in the troposphere and stratosphere, *J. Geophys. Res.*, *107*, 10.1029/2001JD000891, in press, 2002.

Müller, R., P. J. Crutzen, J.-U. Grooss, C. Brühl, J. M. Russell III, and A. F. Tuck, Chlorine activation and ozone depletion in the Arctic vortex: Observations by the Halogen Occultation Experiment on the Upper Atmosphere Research Satellite, *J. Geophys. Res.*, *101*, 12,531–12,554, 1996.

Müller, R., J.-U. Grooss, D. S. McKenna, P. J. Crutzen, C. Brühl, J. M. Russell III, and A. F. Tuck, HALOE observations of the vertical structure of chemical ozone depletion in the Arctic vortex during winter and early spring 1996–1997, *Geophys. Res. Lett.*, *24*, 2717–2720, 1997.

Nash, E. R., P. A. Newman, J. E. Rosenfield, and M. R. Schoeberl, An objective determination of the polar vortex using Ertel's potential vorticity, *J. Geophys. Res.*, *101*, 9471–9478, 1996.

National Oceanic and Atmospheric Administration (NOAA), *Northern Hemisphere Winter Summary 1999–2000*, edited by M. Gelman, Natl. Oceanic and Atmos. Admin., Silver Spring, Md., Apr. 2000. (Available at www.cpc.ncep.noaa.gov/products/stratosphere/winter_bulletins/nh_99-00/index.html.).

Newman, P. A., et al., An overview of the SOLVE/THESEO 2000 campaign, *J. Geophys. Res.*, *107*, 10.1029/2001JD001303, in press, 2002.

Pierce, R. B., et al., Large-scale chemical evolution of the Arctic vortex during the 1999–2000 winter: HALOE/POAM3 Lagrangian photochemical modeling for the SAGE III ozone loss and validation experiment (SOLVE) campaign, *J. Geophys. Res.*, *107*, 10.1029/2001JD001063, in press, 2002.

Plumb, R. A., D. W. Waugh, and M. P. Chipperfield, The effects of mixing on tracer relationships in the polar vortices, *J. Geophys. Res.*, *105*, 10,047–10,062, 2000.

Ray, E. A., F. L. Moore, J. W. Elkins, D. F. Hurst, P. A. Romashkin, G. S. Dutton, and D. W. Fahey, Descent and mixing in the 1999/2000 northern polar vortex inferred from in situ tracer measurements, *J. Geophys. Res.*, *107*, 10.1029/2001JD000961, in press, 2002.

Rex, M., et al., Chemical depletion of Arctic ozone in winter 1999/2000, *J. Geophys. Res.*, *107*, 10.1029/2001JD000533, in press, 2002.

Romashkin, P. A., D. F. Hurst, J. W. Elkins, G. S. Dutton, D. W. Fahey, R. E. Dunn, F. L. Moore, R. C. Myers, and B. D. Hall, In situ measurements of long-lived trace gases in the lower stratosphere by gas chromatography, *J. Atmos. Oceanic Tech.*, *18*, 1195–1204, 2001.

Rosenfield, J. E., P. A. Newman, and M. R. Schoeberl, Computations of diabatic descent in the stratospheric polar vortex, *J. Geophys. Res.*, *99*, 16,677–16,689, 1994.

Russell, J. M., III, A. F. Tuck, L. L. Gordley, J. H. Park, S. R. Drayson, J. E. Harries, R. J. Cicerone, and P. J. Crutzen, HALOE Antarctic observations in the spring of 1991, *Geophys. Res. Lett.*, *20*, 719–722, 1993a.

Russell, J. M., III, L. L. Gordley, J. H. Park, S. R. Drayson, W. D. Hesketh, R. J. Cicerone, A. F. Tuck, J. E. Frederick, J. E. Harries, and P. J. Crutzen, The Halogen Occultation Experiment, *J. Geophys. Res.*, *98*, 10,777–10,797, 1993b.

Salawitch, R. J., et al., Chemical loss of ozone during the Artic winter of 1999/2000: An analysis based on balloon-borne observations, *J. Geophys. Res.*, *107*, 8269, doi:10.1029/2001JD000620, 2002.

Schauffler, S. M., E. L. Atlas, D. R. Blake, F. Flocke, R. A. Lueb, J. M. Lee-Taylor, V. Stroud, and W. Travnicek, Distributions of brominated organic compounds in the troposphere and lower stratosphere, *J. Geophys. Res.*, *104*, 21,513–21,535, 1999.

Schmidt, U., G. Kulessa, G. Klein, E.-P. Röth, P. Fabian, and R. Borchers, Intercomparison of balloon-borne cryogenic whole air samplers during the MAP/GLOBUS 1983 campaign, *Planet. Space Sci.*, *35*, 647–656, 1987.

Schmidt, U., R. Bauer, A. Khedim, E. Klein, G. Kulessa, and C. Schiller, Profile observations of long-lived trace gases in the Arctic vortex, *Geophys. Res. Lett.*, *18*, 767–770, 1991.

Schoeberl, M. R., and D. L. Hartmann, The dynamics of the stratospheric polar vortex and its relation to springtime ozone depletions, *Science*, *251*, 46–52, 1991.

Schoeberl, M. R., L. R. Lait, P. A. Newman, and J. E. Rosenfield, The structure of the polar vortex, *J. Geophys. Res.*, *97*, 7859–7882, 1992.

Schoeberl, M. R., M. Luo, and J. E. Rosenfield, An analysis of the Antarctic Halogen Occultation Experiment trace gas observations, *J. Geophys. Res.*, *100*, 5159–5172, 1995.

Scott, S. G., T. P. Bui, K. R. Chan, and S. W. Bowen, The meteorological measurement system on the NASA ER-2 aircraft, *J. Atmos. Oceanic Tech.*, *7*, 525–540, 1990.

Stachnik, R., J. C. Hardy, J. A. Tarsala, J. W. Waters, and N. R. Erickson, Submillimeter wave heterodyne measurements of stratospheric ClO, HCl, O_3 and HO_2: First results, *Geophys. Res. Lett.*, *19*, 1931–1934, 1992.

Stiller, G. P., M. R. Gunson, L. L. Lowes, M. C. Abrams, O. F. Raper, C. B. Farmer, R. Zander, and C. P. Rinsland, Stratospheric and mesospheric pressure-temperature profiles from rotational analysis of CO_2 lines in atmospheric trace molecule spectroscopy/ATLAS 1 infrared solar occultation spectra, *J. Geophys. Res.*, *100*, 3107–3117, 1995.

Strahan, S. E., J. E. Rosenfield, M. Loewenstein, J. R. Podolske, and A. Weaver, Evolution of the 1991–1992 Arctic vortex and comparison with the Geophysical Fluid Dynamics Laboratory SKYHI general circulation model, *J. Geophys. Res.*, *99*, 20,713–20,723, 1994.

Strahan, S. E., J. E. Nielsen, and M. C. Cerniglia, Long-lived tracer transport in the Antarctic stratosphere, *J. Geophys. Res.*, *101*, 26,615–26,629, 1996.

Swinbank, R., and A. O'Neill, A stratosphere-troposphere data assimilation system, *Mon. Weather Rev.*, *122*, 686–702, 1994.

Toon, G. C., The JPL MkIV Interferometer, *Opt. Photonics News*, *2*, 19–21, 1991.

Toon, G. C., C. B. Farmer, L. L. Lowes, P. W. Schaper, J.-F. Blavier, and R. H. Norton, Infrared aircraft measurements of stratospheric composition over Antarctica during September 1987, *J. Geophys. Res.*, *94*, 16,571–16,596, 1989.

Toon, G. C., C. B. Farmer, P. W. Schaper, L. L. Lowes, R. H. Norton, M. R. Schoeberl, L. R. Lait, and P. A. Newman, Evidence for subsidence in the 1989 Arctic winter stratosphere from airborne infrared composition measurements, *J. Geophys. Res.*, *97*, 7963–7970, 1992.

Toon, G. C., et al., Comparison of MkIV balloon and ER-2 aircraft measurements of atmospheric trace gases, *J. Geophys. Res.*, *104*, 26,779–26,790, 1999.

Traub, W. A., K. W. Jucks, D. G. Johnson, and K. V. Chance, Subsidence of the Arctic stratosphere determined from thermal emission of hydrogen fluoride, *J. Geophys. Res.*, *100*, 11,261–11,267, 1995.

Vömel, H., S. J. Oltmans, D. J. Hofmann, T. Deshler, and J. M. Rosen, The evolution of the dehydration in the Antarctic stratospheric vortex, *J. Geophys. Res.*, *100*, 13,919–13,926, 1995.

von König, M., H. Bremer, V. Eyring, A. P. H. Goede, H. Hetzheim, Q. L. Kleipool, H. Küllmann, and K. Künzi, An airborne submillimeter radiometer for the observation of stratospheric trace gases, in *Microwave Radiometry and Remote Sensing of the Earth's Surface and Atmosphere*, edited by P. Pampaloni and S. Paloscia, pp. 409–415, VSP, Utrecht, Netherlands, 2000.

Waugh, D. W., and W. J. Randel, Climatology of Arctic and Antarctic polar vortices using elliptical diagnostics, *J. Atmos. Sci.*, *56*, 1594–1613, 1999.

Waugh, D. W., and P.-P. Rong, Interannual variability in the decay of lower stratospheric Arctic vortices, *J. Meteor. Soc.*, in press, 2002.

Waugh, D. W., W. J. Randel, S. Pawson, P. A. Newman, and E. R. Nash, Persistence of the lower stratospheric polar vortices, *J. Geophys. Res.*, *104*, 27,191–27,201, 1999.

Webster, C. R., R. D. May, C. A. Trimble, R. G. Chave, and J. Kendall, Aircraft (ER-2) Laser Infrared Absorption Spectrometer (ALIAS) for in situ stratospheric measurements of HCl, N_2O, CH_4, NO_2, and HNO_3, *Appl. Opt.*, *33*, 454–472, 1994.

E. Atlas and S. M. Schauffler, NCAR, P.O. Box 3000, Boulder, CO 80307, USA. (atlas@acd.ucar.edu; sues@ucar.edu)

J.-F. Balvier, R. L. Herman, B. Sen, R. A. Stachnik, G. C. Toon, and C. R. Webster, Jet Propulsion Laboratory, 4800 Oak Grove Drive, MS 183-601, Pasadena, CA 91109-8099, USA. (Jeanfrancois.L.Blavier@jpl.nasa.gov; Robert.L.Herman@jpl.nasa.gov; bhaswar.sen@jpl.nasa.gov; Robert.A.Stachnik@jpl.nasa.gov; Geoffrey.C.Toon@jpl.nasa.gov; Chris.R.Webster@jpl.nasa.gov)

H. Bremer and B.-M. Sinnhuber, Institute of Environmental Physics, University of Bremen, P.O. Box 330440, D-28334 Bremen, Germany. (bremer@iup.physik.uni-bremen.de; bms@iup.physik.uni-bremen.de)

T. P. Bui, H.-J. Jost, M. Loewenstein, and J. R. Podolske, NASA Ames Research Center, MS 245-5, Moffett Field, CA 94035, USA. (pbui@mail.arc.nasa.gov; hjost@mail.arc.nasa.gov; mloewenstein@mail.arc.nasa.gov; jpodolske@mail.arc.nasa.gov)

M. Chipperfield, School of the Environment, University of Leeds, Leeds, LS2 9JT, UK. (martyn@env.leeds.ac.uk)

J. W. Elkins, D. F. Hurst, F. L. Moore, S. J. Oltmans, and H. Vömel, NOAA/CMDL, 325 Broadway, MS R/CMDL1, Boulder, CO 80305, USA. (James.W.Elkins@noaa.gov; Dale.Hurst@noaa.gov; Fred.Moore@noaa.gov; samuel.j.oltmans@noaa.gov; Holger.Voemel@noaa.gov)

A. Engel, M. Müller, and U. Schmidt, Senckenberganlage 32, (PF 194), Institute for Meteorology and Geophysics, Box 19 32, D-60054 Frankfurt am Main, Germany. (an.engel@meteor.uni-frankfurt.de; m.mueller@meteor.uni-frankfurt.de; u.schmidt@meteor.uni-frankfurt.de)

J. B. Greenblatt, Program in Atmospheric and Oceanic Sciences, Princeton University, P. O. Box CN710, Sayre Hall, Princeton, NJ 08544-0710, USA. (buygreen@splash.princeton.edu)

F. Lefèvre, Université Pierre et Marie Curie, BP 102, 4 Place Jussieu, F-75252 Paris Cedex 05, France. (franck.lefevre@aero.jussieu.fr)

R. B. Pierce, NASA Langley Research Center, MS 401B, Hampton, VA 23681, USA. (r.b.pierce@larc.nasa.gov)

E. A. Ray, NOAA Aeronomy Laboratory, 325 Broadway, MS R/AL6, Boulder, CO 80303, USA. (eray@al.noaa.gov)